Vascular endothelium plays a key role in directing pulmonary epithelial cell differentiation

Jiayi Yao,[1] Pierre J. Guihard,[1] Xiuju Wu,[1] Ana M. Blazquez-Medela,[1] Melissa J. Spencer,[2] Medet Jumabay,[1] Peter Tontonoz,[3,5,6] Alan M. Fogelman,[4] Kristina I. Boström,[1,6] and Yucheng Yao[1,7]

[1]Division of Cardiology, [2]Department of Neurology, [3]Department of Pathology and Laboratory Medicine, and [4]Department of Medicine, David Geffen School of Medicine, University of California, Los Angeles, Los Angeles, CA
[5]Department of Pathology and Laboratory Medicine, Howard Hughes Medical Institute, [6]Molecular Biology Institute, and [7]Jonsson Comprehensive Cancer Center, University of California, Los Angeles, Los Angeles, CA

The vascular endothelium is critical for induction of appropriate lineage differentiation in organogenesis. In this study, we report that dysfunctional pulmonary endothelium, resulting from the loss of matrix Gla protein (MGP), causes ectopic hepatic differentiation in the pulmonary epithelium. We demonstrate uncontrolled induction of the hepatic growth factor (HGF) caused by dysregulated cross talk between pulmonary endothelium and epithelium in *Mgp*-null lungs. Elevated HGF induced hepatocyte nuclear factor 4 α (Hnf4a), which competed with NK2 homeobox 1 (Nkx2.1) for binding to forkhead box A2 (Foxa2) to drive hepatic differentiation in *Mgp*-null airway progenitor cells. Limiting endothelial HGF reduced Hnf4a, abolished interference of Hnf4a with Foxa2, and reduced hepatic differentiation in *Mgp*-null lungs. Together, our results suggest that endothelial–epithelial interactions, maintained by MGP, are essential in pulmonary cell differentiation.

Introduction

In recent years, several studies have demonstrated the important role of vascular endothelium in endothelial–epithelial interactions during the developmental process (Matsumoto et al., 2001; Ding et al., 2010, 2011; Lee et al., 2014). Endothelial cells (ECs) direct proliferation and differentiation of epithelial cells (Lee et al., 2014), whereas epithelial cells stimulate ECs to proliferate and form blood vessels. Indeed, inductive effects of ECs on epithelial differentiation have been identified during the development of lungs, liver, heart, pancreas, stomach, and bone (Matsumoto et al., 2001; Ding et al., 2010, 2011; Kusumbe et al., 2014), and the absence of ECs results in defective development of the liver bud (Matsumoto et al., 2001).

The pulmonary vasculature exhibits unique characteristics to allow for gas exchange. The pulmonary endothelium coordinates with the epithelium to form alveolar units, where cell–cell contact facilitates the endothelial–epithelial interactions in the peripheral respiratory system. Pulmonary ECs have been shown to not only support pulmonary epithelial cells, but also to guide the differentiation and maturation of epithelial cells (Ding et al., 2011). The absence of ECs results in incomplete induction of pulmonary lineages in pulmonary progenitor cells (Lee et al., 2014), and endothelial defects may impair epithelial repair after lung injury (Lee et al., 2014).

Matrix Gla protein (MGP), a bone morphogenetic protein (BMP) antagonist (Zebboudj et al., 2002; Yao et al., 2008, 2011), is best known for its ability to prevent calcification in elastic arteries (Luo et al., 1997; Speer et al., 2009) but is also highly expressed in pulmonary epithelial cells (Gilbert and Rannels, 2004; Yao et al., 2007, 2011). Excessive MGP in mice inhibits pulmonary vascular growth by limiting BMP activity and VEGF expression (Yao et al., 2007, 2011), and mutations in the human *Mgp* gene, known as the Keutel syndrome, cause peripheral pulmonary stenosis and other developmental defects (Meier et al., 2001). We previously demonstrated that deletion of the *Mgp* gene in mice causes an imbalance between the pulmonary vasculature and the airways, leading to vascular overgrowth with arteriovenous malformation and underdeveloped airways (Yao et al., 2011). Furthermore, MGP is necessary to ensure normal endothelial differentiation in progenitor cells (Yao et al., 2016) and prevent arterial ECs from undergoing endothelial–mesenchymal transitions (Yao et al., 2013a, 2015).

We now report that MGP is essential for endothelial–epithelial interactions to direct pulmonary specification. The absence of MGP disrupts such interactions and triggers hepatic differentiation in the pulmonary epithelium as mediated by the

Correspondence to Yucheng Yao: yyao@mednet.ucla.edu; Kristina I. Boström: kbostrom@mednet.ucla.edu

Abbreviations used: AF, Alexa Fluor; AFP, α-fetoprotein; BMP, bone morphogenetic protein; CCSP, Clara cell marker of Clara cell secretory protein; ChIP, chromatin immunoprecipitation; EC, endothelial cell; ESC, embryonic stem cell; HGF, hepatic growth factor; MGP, matrix Gla protein; PE, phycoerythrin; VE, vascular endothelial; WB, wash buffer.

The Rockefeller University Press
J. Cell Biol. Vol. 216 No. 10 3369–3385
https://doi.org/10.1083/jcb.201612122

endothelium. Our results highlight the importance of the cross talk between endothelium and epithelium in pulmonary specification and suggest that timely MGP expression is essential to suppress hepatic differentiation in the lungs. It also explains the near absence of MGP expression in the liver.

Results

Hepatic differentiation in *Mgp*$^{-/-}$ lungs

Because multiple organs in *Mgp*$^{-/-}$ mice have highly abnormal phenotypes (Yao et al., 2007, 2011, 2013a,b), we analyzed the global gene expression profiles derived from different organs in these mice. Unexpectedly, we found that the lung profile clustered closely with that of the liver (Fig. 1 a). In the *Mgp*$^{-/-}$ lungs, gene expression involved in the metabolism of fat, glucose and cholesterol, cytochromes, xenobiotics, and hepatic enzymes was similar to that of *Mgp*$^{-/-}$ and *Mgp*$^{+/+}$ liver (Fig. 1 b). We confirmed these changes in the early hepatocyte markers albumin, GATA-binding protein 4 (Gata4), forkhead box A3 (Foxa3), HNF1 homeobox A (Hnf1a), hepatocyte nuclear factor 4 α (Hnf4a), α-fetoprotein (AFP), the hematopoietically expressed homeobox (Hex), and hepatic growth factor (HGF), as well as the mature hepatocyte markers transthyretin (Ttr), phenylalanine hydroxylase (Pah), and apolipoproteins (Fig. 1, c and d; and Fig. S1 a). The results showed that all of these markers were induced in the *Mgp*$^{-/-}$ lungs. In addition, high levels of albumin protein (Fig. 1 e) and cytochrome P450 activity (Fig. 1 f), which are normal findings in liver (Sekiya and Suzuki, 2011), were observed in isolated *Mgp*$^{-/-}$ lung cells. As might be expected, disordered alveolar structure with abnormal cell mixtures was detected in the *Mgp*$^{-/-}$ lungs by transmission EM (Fig. S1 b). Together, the results suggest the occurrence of ectopic hepatic differentiation in *Mgp*$^{-/-}$ lungs. Expression of MGP in normal liver is extremely low, and no significant changes in expression profiles or hepatocytes were detected in *Mgp*$^{-/-}$ liver as compared with normal liver (Fig. 1 a; Luo et al., 1997). We did not detect any induction of pulmonary markers in the livers of *Mgp*$^{tg/wt}$ mice (Fig. S2), in which excess human MGP was expressed (Yao et al., 2007). However, gene expression associated with lung function differed between *Mgp*$^{-/-}$ and *Mgp*$^{+/+}$ lungs (Fig. 1 b), consistent with our previous findings (Yao et al., 2007, 2011). Pathological examination excluded tumorigenesis in all of the examined *Mgp*$^{-/-}$ lungs.

We performed lineage tracing to further investigate the hepatic differentiation in *Mgp*$^{-/-}$ lungs. We traced albumin expression in the lungs of *Mgp*$^{-/-}$ and *Mgp*$^{+/+}$ mice using *Alb*^{Cre}*Rosa*^{LacZ} and *Alb*^{Cre}*Rosa*^{EGfp} transgenic mice, where Cre-activated expression of β-galactosidase or EGFP is driven by the albumin promoter (Fig. 1, g and h; Postic et al., 1999; Soriano, 1999; Ballarín-González et al., 2013). We observed high pulmonary expression of β-galactosidase in *Alb*^{Cre}*Rosa*^{LacZ}*Mgp*$^{-/-}$ mice at 4 wk of age (Fig. 1 h) and EGFP in *Alb*^{Cre}*Rosa*^{EGfp}*Mgp*$^{-/-}$ mice on embryonic day (E) 13.5 and postnatal day (P) 28 (Fig. 1 i and Fig. S3). The expression of EGFP was confirmed by flow cytometric analysis (Fig. 1 j).

We examined the pulmonary function of *Mgp*$^{-/-}$ mice by unrestricted whole body barometric plethysmography. We found that the respiratory rate of *Mgp*$^{-/-}$ mice was >1.5-fold higher than that of WT mice during room air breathing and in the hypercapnia phase, whereas no significant difference in tidal volume was detected between *Mgp*$^{-/-}$ and WT mice. We found a significant increase of peak expiratory and inspiratory flow and minute ventilation in *Mgp*$^{-/-}$ mice during room air breathing. Together, the data suggested the increased respiration in *Mgp*$^{-/-}$ mice (Fig. 1 k). We also examined the expression of the pulmonary marker NK2 homeobox 1 (Nkx2.1), the type I pulmonary epithelial marker aquaporin 5 (Aqp5), the type II pulmonary epithelial marker surfactant-associated protein B and C (Spb and Spc), and the Clara cell marker of Clara cell secretory protein (CCSP) using real-time PCR. The result showed a significant decrease in CCSP in *Mgp*$^{-/-}$ lungs (Fig. 1 l), suggesting a disruption of epithelial cell differentiation. Our previous study showed no difference in arterial oxygen levels between *Mgp*$^{-/-}$ and WT mice (Yao et al., 2013b). We argue that the enhanced respiration in *Mgp*$^{-/-}$ mice compensates for the inefficiency of gas exchange caused by abnormal epithelial cell differentiation.

We also examined albumin expression in organs with variable levels of MGP expression (Yao et al., 2007) including lungs, artery, brain, kidneys, bone, heart, muscle, and liver. The albumin expression was only increased in the *Mgp*$^{-/-}$ lungs (Fig. 1 m).

Hepatic differentiation in *Mgp*$^{-/-}$ airway progenitors

To understand how hepatic differentiation occurs in *Mgp*$^{-/-}$ lungs, we first identified MGP in the epithelium of embryonic lungs from E12.5 to E18.5 by immunofluorescence (Fig. 2 a). To determine what cells were responsible for the MGP expression, we separated pulmonary ECs and epithelial cells using flow cytometry with antibodies recognizing the endothelial marker CD31 and examined MGP expression by real-time PCR. The results revealed that MGP expression was significantly higher in the CD31^{-} pulmonary cells than in the CD31^{+} pulmonary ECs (Fig. 2 b). Furthermore, in *Mgp*$^{-/-}$ lungs, the hepatic markers Foxa3, Gata4, Hnf4a, albumin, and c-Met were all increased in the CD31^{-} cell population, whereas HGF and Flt1 were abnormally induced in the CD31^{+} ECs (Fig. 2 c). No MGP was detected in the liver of *Mgp*$^{+/+}$ or *Mgp*$^{-/-}$ mice (Fig. 2, b–d).

To further investigate whether hepatic differentiation occurred in *Mgp*$^{-/-}$ pulmonary cells, we successfully isolated a large population of cells that expressed albumin and AFP from P28 *Mgp*$^{-/-}$ lungs by flow cytometry (Fig. 3 a). We examined hepatic, pulmonary epithelial, and endothelial markers by real-time PCR. The hepatocyte markers Ttr, Foxa3, and Hnf4a were highly induced in these cells, as well as the pulmonary epithelial markers Nkx2.1, Aqp5, and CCSP and Spb, Spc, and Spd. However, no significant expression of the endothelial markers Flk1, vascular endothelial (VE)–cadherin, and CD31 was detected (Fig. 3 b), suggesting that hepatic differentiation occurred only in the *Mgp*$^{-/-}$ pulmonary epithelial cells.

To determine which pulmonary cell lineage expressed the hepatic markers, we first costained albumin with the airway progenitor markers Sox9 and Foxp2 (Mou et al., 2012) in E12.5 embryonic lungs from *Mgp*$^{+/+}$ and *Mgp*$^{-/-}$ mice. The results revealed that albumin was expressed in the Sox9^{+}Foxp2^{+} airway progenitors in *Mgp*$^{-/-}$ lungs (Fig. 3 c). We then determined whether albumin was expressed in cells normally derived from these progenitors by costaining albumin and pulmonary epithelial cell markers in P28 *Mgp*$^{-/-}$ lungs: Spb for type II epithelial cells, Aqp5 for type I epithelial cells, and CCSP for Clara cells. We found that albumin colocalized with all three markers (Fig. 3 d), suggesting that hepatic differentiation was triggered

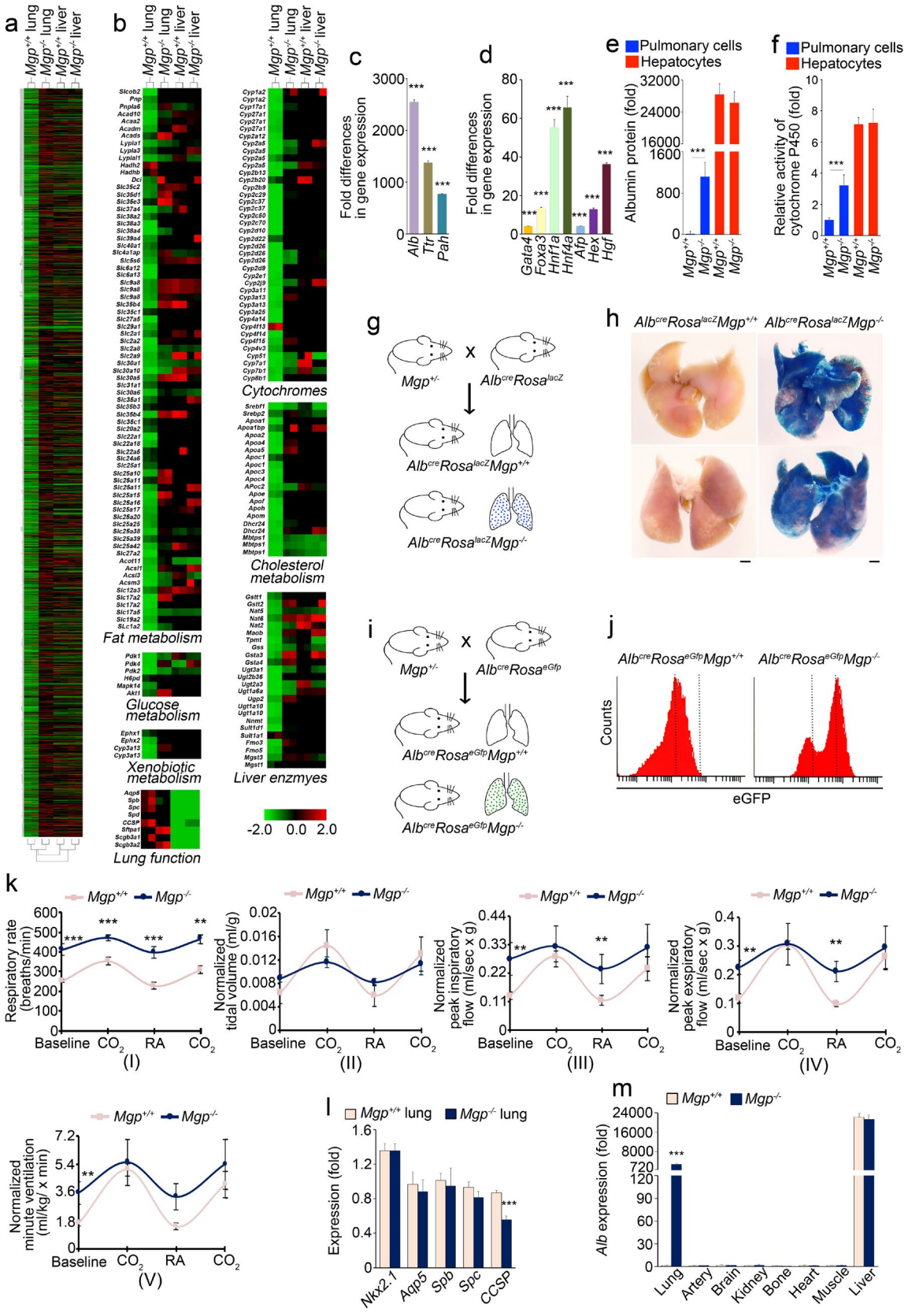

Figure 1. **Hepatic differentiation in the lungs of *Mgp*$^{-/-}$ mice.** (a) Gene expression profiles from lungs and liver of WT (*Mgp*$^{+/+}$) and *Mgp*$^{-/-}$ mice (n = 2). (b) Genes involved in liver metabolism with extraction of significant difference in expression ($P < 0.05$). (c and d) Expression of select hepatic markers was analyzed by real-time PCR. The difference in expression was calculated as a fold change as compared between *Mgp*$^{+/+}$ and *Mgp*$^{-/-}$ lungs (n = 10). (e and f) Albumin levels (e) and activity of P450 (f) were compared in cells isolated from *Mgp*$^{+/+}$ and *Mgp*$^{-/-}$ lungs. Isolated hepatocytes from *Mgp*$^{+/+}$ and *Mgp*$^{-/-}$ liver were used as controls (n = 8). (g) Schematic diagram of strategy for detecting albumin promoter–driven expression of β-galactosidase (LacZ)

early in airway progenitor cells and maintained in $Mgp^{-/-}$ pulmonary epithelium (Fig. 3 e).

Interestingly, expression of HGF was significantly higher in the albumin and AFP-negative cells (Fig. 3 b), supporting that HGF was induced in $Mgp^{-/-}$ pulmonary ECs. For validation, we costained HGF and the early endothelial marker CD34 in $Mgp^{-/-}$ lung from E12.5 to E18.5 and found colocalization of HGF with CD34 (Fig. 4 a), but not with Nkx2.1 (Fig. 4 b). These results confirmed the induction of HGF in $Mgp^{-/-}$ pulmonary ECs.

Endothelial-specific gene deletion of Hgf decreases hepatic differentiation in $Mgp^{-/-}$ lungs

To determine the role of endothelial HGF in the ectopic differentiation in $Mgp^{-/-}$ lungs, we used $Cdh5^{Cre}$ mice where Cdh5 (VE-cadherin) promoter–driven Cre is expressed in ECs (Alva et al., 2006). We crossbred $Cdh5^{Cre}$ and $Hgf^{flox/flox}$ mice with $Mgp^{+/-}$ mice to obtain $Chd5^{Cre}Hgf^{flox/flox}Mgp^{-/-}$ mice with EC-specific deletion of *Hgf* (Fig. 5 a). The mice still exhibited the $Mgp^{-/-}$ phenotype with vascular calcification as previously described (Luo et al., 1997; Yao et al., 2011, 2013b), suggesting that depletion of HGF had no additional effect on the vasculature.

We then examined the expression of genes related to metabolism of fat, glucose and cholesterol, cytochromes, xenobiotic metabolism, and hepatic enzymes. We found that the similarities in expression between lungs and liver were significantly reduced in $Chd5^{Cre}Hgf^{flox/flox}Mgp^{-/-}$ mice (Fig. 5 b). Furthermore, we examined the expression of the hepatocyte markers albumin, Ttr, Pah, and AFP, the activity of cytochrome P450, and the protein levels of albumin in lungs. Compared with the $Mgp^{-/-}$ lungs, all of these parameters were reduced in the lungs of $Chd5^{Cre}Hgf^{flox/flox}Mgp^{-/-}$ mice (Fig. 5, c and d), suggesting that depletion of endothelial HGF limited ectopic hepatic differentiation in $Mgp^{-/-}$ lungs.

VEGF and Flt1 induces endothelial HGF in $Mgp^{-/-}$ lungs

Our previous studies showed that increased BMP signaling, specifically involving BMP-4, affected pulmonary vascularization and alveolar development in $Mgp^{-/-}$ mice (Yao et al., 2007, 2011). To determine whether dysregulated endothelial–epithelial interactions caused by MGP deficiency induced HGF, we isolated $Mgp^{+/+}$ and $Mgp^{-/-}$ pulmonary epithelial cells and ECs and treated them with 40 ng/ml BMP-4 for 24 h. In $Mgp^{-/-}$ epithelial cells, BMP-4 enhanced the induction of VEGF and c-Met (Fig. 6 a, control), whereas in $Mgp^{-/-}$ ECs, BMP-4 enhanced the induction of Flt1 and HGF (Fig. 6 b, control). We then transfected both cell types with Flt1 siRNA or treated the cells with anti-VEGF– or anti–BMP-4–neutralizing antibodies. In $Mgp^{-/-}$ epithelial cells, knockdown of Flt1 or inhibition of VEGF had no effect on the VEGF and c-Met expression induced by BMP-4 (Fig. 6 a). In $Mgp^{-/-}$ ECs, however, knockdown of Flt1 or inhibition of VEGF abolished the induction of HGF (Fig. 6 b). Inhibition of BMP-4 abolished induction of all four factors in both cell types (Fig. 6, a and b). Together, it suggests that BMP-4 induces VEGF and c-Met in epithelial cells and Flt1 in ECs. Enhanced VEGF signaling through Flt1 then induced endothelial HGF, which has been shown to activate epithelial c-Met (Schmidt et al., 1995). Furthermore, we tested the effect of different concentrations of HGF on albumin expression in $Mgp^{-/-}$ pulmonary epithelial cells. The results show that expression of albumin increased in a dose-dependent manner in response to 10–30 ng/ml HGF but plateaued at HGF levels >30 ng/ml (Fig. 6 c). We also treated $Mgp^{-/-}$ pulmonary ECs with 300 ng/ml BMP-2, 100 ng/ml BMP-7, and 10 ng/ml BMP-9 for 24 h and examined the expression of VEGF, Flt1, Hgf, and c-Met. We found no significant induction in these factors, suggesting specificity of BMP-4 and MGP in the interaction between pulmonary epithelium and endothelium (Fig. 6, d–f). Consequently, MGP is able to regulate communication between the epithelium and endothelium by suppressing HGF through inhibition of BMP-4 activity (Fig. 6 g, working model).

$Mgp^{-/-}$ ECs induce albumin expression in $Mgp^{-/-}$ airway progenitor cells

Because albumin was expressed in the $Nkx2.1^{+}Sox9^{+}FoxP2^{+}$ airway progenitor cells, we hypothesized that dysregulated interactions between endothelium and epithelium allow hepatic differentiation in these progenitors. We tested the hypothesis using airway progenitor cells with and without the inclusion of ECs in a strategy schematically shown in Fig. 7 a.

First, we used WT and $Mgp^{-/-}$ embryonic stem cells (ESCs; Yao et al., 2016) to derive definitive endoderm and lung progenitors using previously published protocols (Mou et al., 2012; Lee et al., 2014). The expression of the endoderm markers EpCAM, c-kit, and CXCR4, as determined by flow cytometry, indicated that a small population of definitive endoderm was derived from the $Mgp^{-/-}$ ESCs (Fig. 7 b). We isolated $EpCAM^{+}c\text{-}kit^{+}$ cells and derived them into airway progenitors (Mou et al., 2012), which were recognized by high expression of Nkx2.1, Sox9, and FoxP2 (Fig. 7 c). There was no significant difference in the expression of these markers between $Mgp^{-/-}$ and WT progenitors (Fig. 7 c). We also examined other lineage markers, including FoxN1 for thymus, Pax8 for thyroid, and Pax9 and Tbx1 for pharyngeal pouch endoderm, and found only minimal induction of these markers (Fig. 7 c). In contrast, we found high induction of c-Met in $Mgp^{-/-}$ ESC-derived endoderm, indicating that abnormal HGF/c-Met signaling occurred during the derivation of the endoderm (Fig. 7 g). The results supported the possibility of using ECS-derived airway progenitors to test our hypothesis. We then labeled the $Mgp^{-/-}$ and WT ESCs with albumin promoter–driven mCherry for hepatic tracing.

We introduced two types of ECs into the derivation of airway progenitor cells, ESC-derived ECs (Yao et al., 2016) and yolk sac–derived EC line C166 (Wang et al., 1996). We infected $Mgp^{-/-}$ and WT ESCs with a lentiviral vector containing Flk1 promoter–driven EGFP. We derived ESCs into ECs and isolated $EGFP^{+}$ ECs by flow cytometry. Expression of the endothelial

in the lungs of $Mgp^{-/-}$ mice. (h) 5-bromo-4-chloro-3-indolyl-β-D-galactopyranoside (X-gak) staining of lungs of $Alb^{Cre}Rosa^{LacZ}Mgp^{+/+}$ and $Alb^{Cre}Rosa^{LacZ}Mgp^{-/-}$ mice (n = 3). (i) Schematic diagram of strategy for detecting albumin promoter–driven expression of EGFP in the lungs of $Mgp^{-/-}$ mice. (j) EGFP-positive cell populations in cells isolated from lungs of $Alb^{Cre}Rosa^{eGfp}Mgp^{+/+}$ and $Alb^{Cre}Rosa^{EGFP}Mgp^{-/-}$ mice were assessed by flow cytometric analysis (n = 3). (k) Pulmonary function of $Mgp^{-/-}$ mice (n = 4). CO_2, hypercapnia phase with 7% CO_2, 21% O_2, and balanced N_2. RA, room air. (l) Expression of pulmonary markers in lungs of $Mgp^{-/-}$ mice. $Mgp^{+/+}$ lung was used as control (n = 6). (m) Expression of albumin in lungs, artery, brain, kidneys, bone, heart, muscle, and liver in $Mgp^{-/-}$ mice. $Mgp^{+/+}$ was used as control (n = 6). Data in c–f and k–m were analyzed by two-sided t test. **, P <0.005; ***, P < 0.001. Error bars are standard deviation. Data distribution was assumed to be normal, but this was not formally tested. Bars, 1 mm.

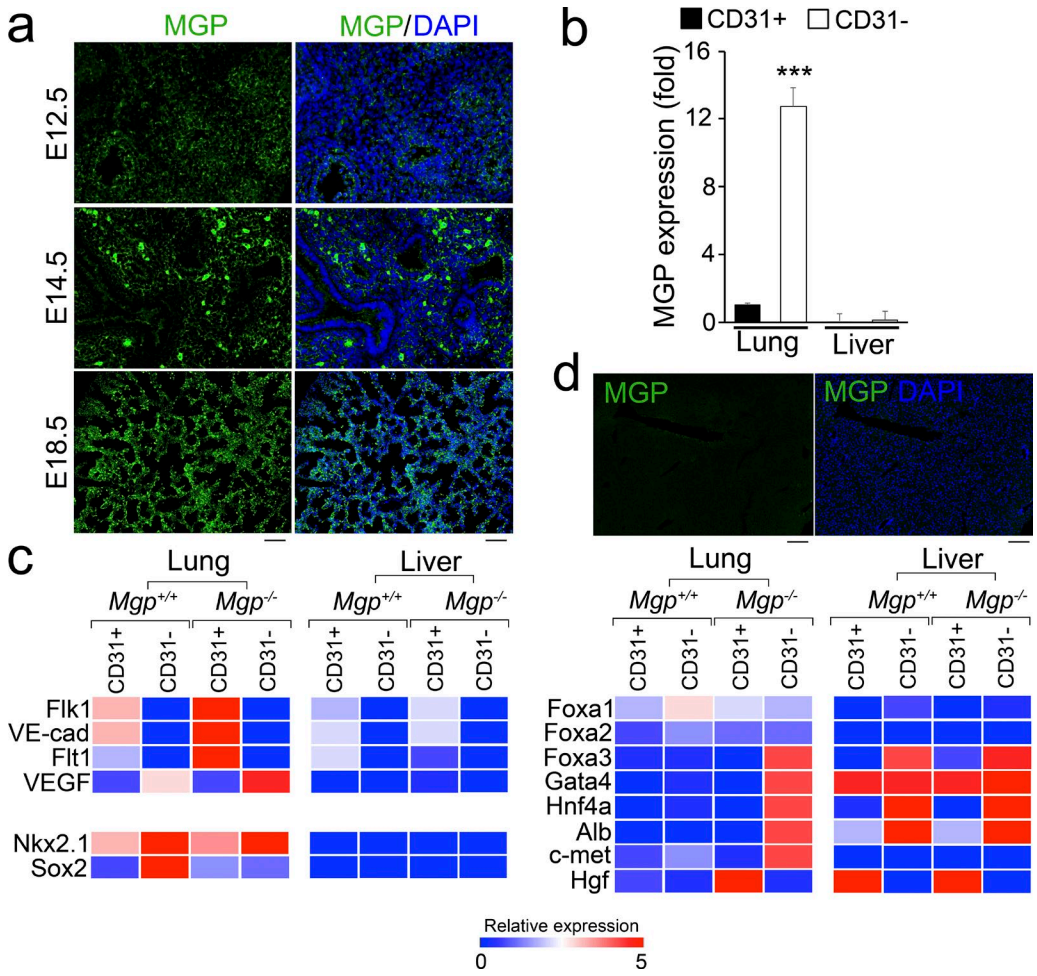

Figure 2. **Expression of MGP, pulmonary endothelial and epithelial makers, and hepatic markers in Cd31⁺ and CD31⁻ pulmonary cells of *Mgp*$^{+/+}$ and *Mgp*$^{-/-}$ mice.** (a) Expression of MGP in embryonic lung from E12.5 to E18.5 ($n = 5$). (b) Expression of MGP in CD31⁺ and CD31⁻ cells isolated from lung and liver ($n = 3$). (c) Relative gene expression in CD31⁺ and CD31⁻ cells isolated from lung and liver in *Mgp*$^{+/+}$ and *Mgp*$^{-/-}$ mice ($n = 3$). (d) Expression of MGP in liver at E18.5 was analyzed by two-sided *t* test. ***, $P < 0.001$. Error bars are standard deviation. Data distribution was assumed to be normal, but this was not formally tested. Bars, 50 µm.

markers VE-cadherin, von Willebrand factor, and CD31 and GFP expression driven by Flk1 promoter were verified in these ECs (Fig. 7, d and e). C166 ECs were used as control cells. We infected the C166 EC line with lentiviral vectors containing EGFP and MGP siRNA and selected EGFP-positive cells with ≥95% of MGP mRNA knockdown (not depicted). We examined the time course of MGP expression during derivation of ECs and definitive endoderm from ESCs. Induction of MGP occurred in both processes, but the MGP level in the definitive endoderm was higher than that in the ECs (Fig. 7 f). We examined expression of HGF, Flt1, and c-Met in both types of ECs and found induction of HGF and Flt1, but not c-Met (Fig. 7, g and h). Subsequently, we included EGFP-labeled ECs into the derivation of airway progenitors from ESC-derived endoderm and examined the expression of albumin at the end of the derivation. We observed that co-culture of *Mgp*$^{-/-}$ ECs with *Mgp*$^{-/-}$ endoderm resulted in high induction of albumin (Fig. 7 i), and albumin was only detected in the airway progenitor cells (Fig. 7 j). No induction of albumin was detected in the co-cultures of *Mgp*$^{+/+}$ ECs with *Mgp*$^{+/+}$ endoderm, *Mgp*$^{+/+}$ ECs with *Mgp*$^{-/-}$ endoderm, or *Mgp*$^{-/-}$ ECs with *Mgp*$^{+/+}$ endoderm (Fig. 7, i and j). We then treated the co-cultures with anti-Flt1– or anti-HGF–neutralizing antibodies, which diminished the induction of albumin (Fig. 7 i), suggesting that the induction of albumin resulted from the induction of Flt1 and HGF in the *Mgp*$^{-/-}$ ECs. We repeated the co-culture experiments with C166 ECs and ESC-derived endoderm with similar results: only MGP-depleted C166 induced albumin expression in *Mgp*$^{-/-}$ airway progenitors (Fig. 7, k–m). The results indicated that the induction of endothelial HGF after activation by VEGF and Flt1 induced hepatic differentiation in pulmonary epithelium.

Induced Hnf4a interacts with Foxa2 in *Mgp*$^{-/-}$ lungs

To investigate possible factors involved in the ectopic hepatic differentiation in *Mgp*$^{-/-}$ lungs, we examined the transcription factors Foxa2, Hnf4a, and Nkx2.1. Hnf4a and Foxa2 are known to interact (Wallerman et al., 2009) and convert mouse embryonic and adult fibroblasts into hepatocyte-like cells (Sekiya and Suzuki, 2011). Nkx2.1 and Foxa2 interact in lung epithelial cells and are associated with the repression of lung adenocarcinoma metastasis (Snyder et al., 2013; Li et al., 2015). We hypothesized that abnormally expressed Hnf4a in *Mgp*$^{-/-}$ lungs interferes with the binding between Nkx2.1 and Foxa2, allowing competitive binding between Hnf4a and Foxa2 to induce hepatic differentiation. To test this hypothesis, we first exam-

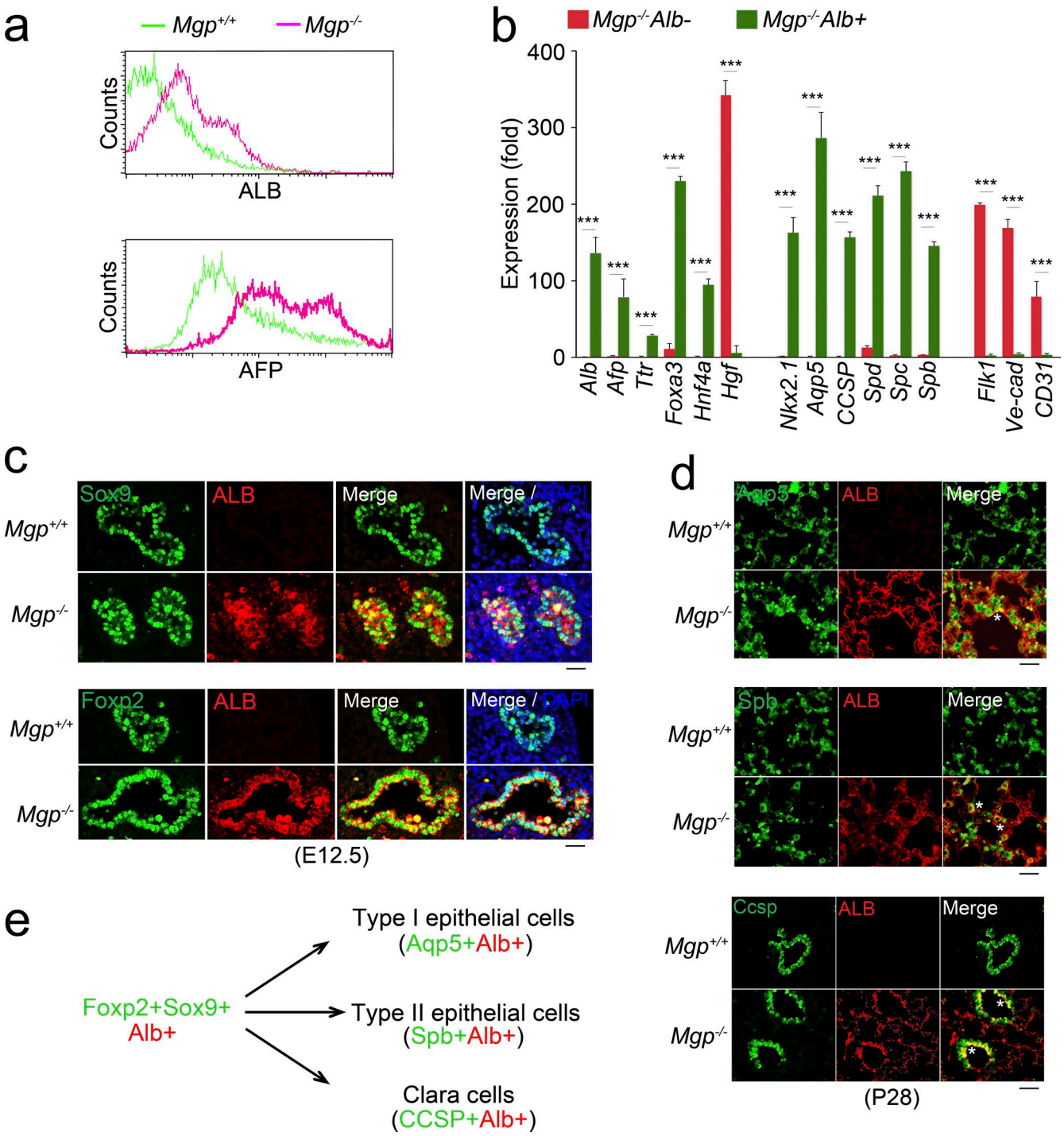

Figure 3. **Hepatic differentiation occurs in the epithelium of *Mgp*$^{-/-}$ lungs.** (a) Analysis of albumin and AFP-positive cells in *Mgp*$^{-/-}$ lungs (n = 3). (b) Gene expression involved in hepatic, pulmonary, or endothelial differentiation was determined in albumin and AFP–double-positive cells in *Mgp*$^{-/-}$ lungs by real-time PCR. Negative cells were used as controls. Data were analyzed by two-sided t test. ***, P < 0.001. Error bars are standard deviation. Data distribution was assumed to be normal, but this was not formally tested. (c) Costaining of albumin (red) and airway progenitor markers Sox9 or Foxp2 (green) in WT (*Mgp*$^{+/+}$) and *Mgp*$^{-/-}$ E12.5 lungs (n = 5). (d) Costaining of albumin (red) and type I epithelial cell marker aquaporin 5 (Aqp5), type II epithelial cell marker surfactant protein B (Spb), or CCSP in *Mgp*$^{+/+}$ and *Mgp*$^{-/-}$ lungs on P28 (n = 5). (e) Schematic diagram of the differentiation of albumin-positive cells in *Mgp*$^{-/-}$ lungs. Bars, 50 µm.

ined these factors in *Mgp*$^{-/-}$ lungs. Compared with WT, Hnf4a was highly induced in *Mgp*$^{-/-}$ lungs (Fig. 8 a), whereas Nkx2.1 and Foxa2 were not (Fig. 8 a). We then tested whether Hnf4a binds to Foxa2 in *Mgp*$^{-/-}$ lungs. Lysates of WT and *Mgp*$^{-/-}$ lungs were immunoprecipitated with anti-Foxa2 antibodies and analyzed by immunoblotting using anti-Hnf4a and anti-Nkx2.1 antibodies, respectively. The results revealed binding between Hnf4a and Foxa2 in *Mgp*$^{-/-}$ lungs, but not in WT lungs, suggesting that this interaction leads to ectopic hepatic differentiation in the lungs (Fig. 8 b). The results also showed that Nkx2.1

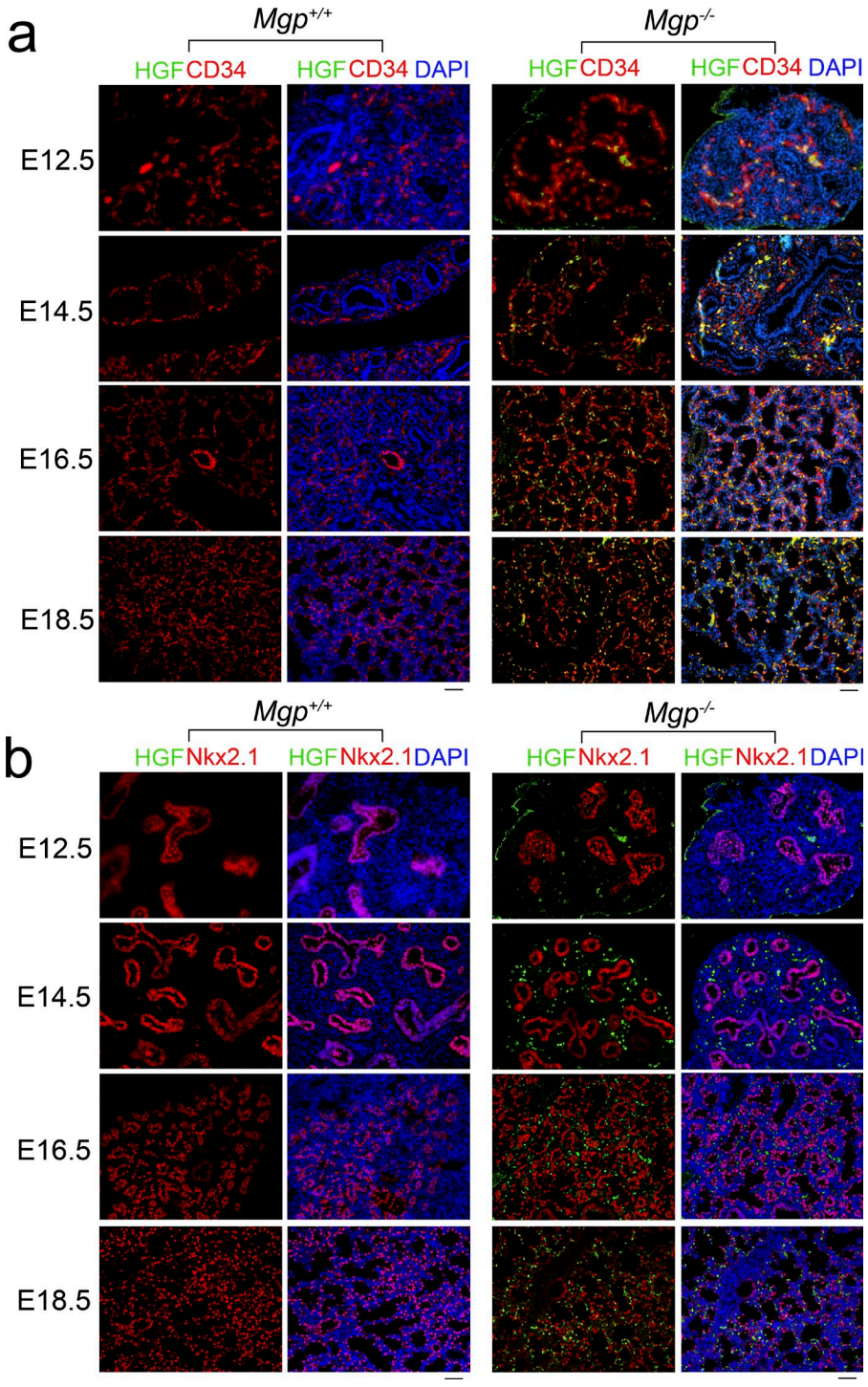

Figure 4. **Expression of endothelial HGF in embryonic lungs.** (a) Costaining of HGF with CD34 in $Mgp^{+/+}$ and $Mgp^{-/-}$ embryonic lungs from E12.5 to E18.5 ($n = 5$). (b) Costaining of HGF with Nkx2.1 in $Mgp^{+/+}$ and $Mgp^{-/-}$ embryonic lungs from E12.5 to E18.5 ($n = 5$). Bars, 50 µm.

bound to Foxa2 in both $Mgp^{-/-}$ and WT lungs, and the binding in $Mgp^{-/-}$ lungs was less than in WT, suggesting that Hnf4a may compete with Nkx2.1 for binding to Foxa2 (Fig. 8 b). To determine whether interactions between Hnf4a and Foxa2 activate hepatic differentiation, we performed chromatin immunoprecipitation (ChIP) assays to examine the albumin locus in $Mgp^{-/-}$ lungs using anti-Hnf4a and anti-Foxa2 antibodies. We found strong binding of Hnf4a and Foxa2 to the two Hnf4a-binding sites in albumin promoter in lysates of $Mgp^{-/-}$ lungs but not in WT controls (Fig. 8, c–e). The Ttr and Pax8 gene promoters were used as positive and negative controls, respectively (Fig. S4; Odom et al., 2004). To determine whether the binding of Hnf4a and Foxa2 affects the transcription state of albumin, we used ChIP assays to assess the balance of bivalent marker methylation of histone H3 lysine 4 (H3K4me3) and histone H3 lysine 27 (H3K27me3) around the Hnf4a-binding site in $Mgp^{-/-}$ lungs. We observed an increase of H3K4me3, which allows gene activation, and a decrease of H3K27me3, which silences genes, supporting transcriptional activation of the albumin gene (Fig. 8 f). We also transfected $Mgp^{-/-}$ epithelial cells with a luciferase construct driven by the albumin promoter and siRNA for Hnf4a or Foxa2. We found that luciferase activity was ele-

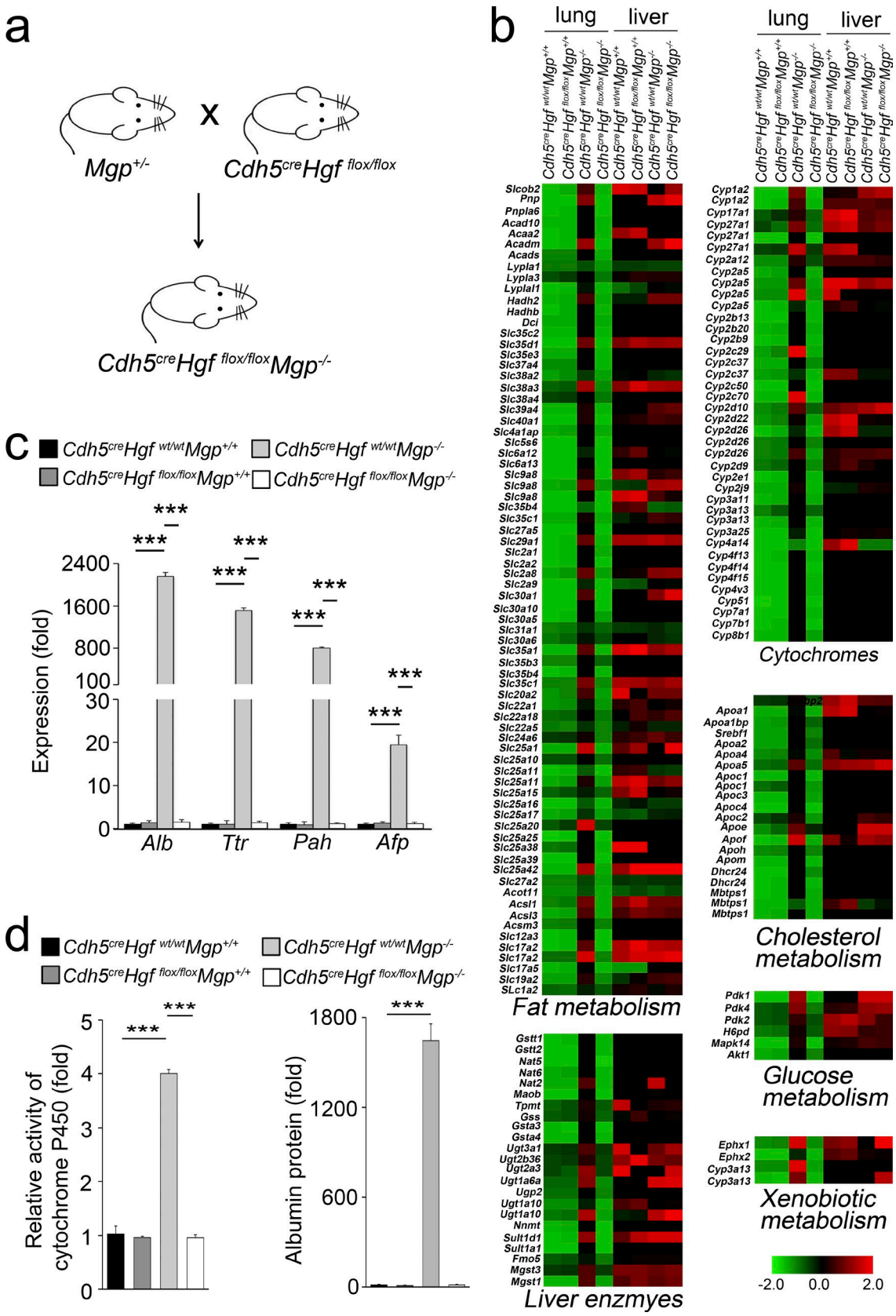

Figure 5. **Decrease of HGF in ECs reduces hepatic differentiation in *Mgp*$^{-/-}$ lungs.** (a) Schematic diagram of breeding strategy to create *Chd5*^{Cre} *Hgf*$^{flox/flox}$*Mgp*$^{-/-}$ mice. (b) Genes involved in liver metabolism, with extraction of significant difference in expression ($P < 0.05$) derived from the gene expression profiles from lungs and liver of *Cdh5*^{Cre}*Hgf*$^{wt/wt}$*Mgp*$^{+/+}$, *Cdh5*^{Cre}*Hgf*$^{flox/flox}$ *Mgp*$^{+/+}$, *Cdh5*^{Cre}*Hgf*$^{wt/wt}$ *Mgp*$^{-/-}$, and *Cdh5*^{Cre}*Hgf*$^{flox/flox}$ *Mgp*$^{-/-}$ mice

vated in $Mgp^{-/-}$ pulmonary epithelial cells and that Hnf4a or Foxa2 siRNA abolished this increase (Fig. 8 g). Together, the results suggest that the interaction between Hnf4a and Foxa2 activates hepatic differentiation in $Mgp^{-/-}$ lungs.

Hnf4a is known to be induced by HGF during liver development (Chen et al., 2005; Hasuike et al., 2005). To determine whether endothelial depletion of HGF affects Hnf4a, we examined the expression of Hnf4a in the lungs of $Chd5^{Cre}Hgf^{flox/flox}Mgp^{-/-}$ by immunoblotting. The results revealed a reduction of Hnf4a (Fig. 8 h), suggesting that the depletion of HGF abolished abnormal induction of Hnf4a in $Mgp^{-/-}$ lungs. We also analyzed lung lysates of $Chd5^{Cre}Hgf^{flox/flox}Mgp^{-/-}$ mice by immunoprecipitation with anti-Foxa2 antibodies. There was no binding between Hnf4a and Foxa2 in the $Chd5^{Cre}Hgf^{flox/flox}Mgp^{-/-}$ mice, and binding between Foxa2 and Nkx2.1 did not differ between WT and $Chd5^{Cre}Hgf^{flox/flox}Mgp^{-/-}$ mice (Fig. 8 i). The results suggested that limiting Hnf4a by depletion of HGF in ECs abolished the binding between Hnf4a and Foxa2 and reduced ectopic hepatic differentiation in the lungs of $Chd5^{Cre}Hgf^{flox/flox}Mgp^{-/-}$ mice (Fig. 8 j). Collectively, our data suggest that cross talk between pulmonary ECs and epithelial cells is essential for directing pulmonary differentiation and that timely MGP expression is critical to prevent hepatic differentiation during lung development.

Discussion

In this study, we identify a critical step in which MGP is required for epithelial–endothelial interactions that are instrumental in suppressing ectopic hepatic differentiation in developing pulmonary epithelium. *Mgp* gene deletion caused a mixed pulmonary and hepatic differentiation in $Mgp^{-/-}$ lungs caused by the loss of BMP inhibition normally provided by MGP, most likely during the pulmonary specification from the foregut. Loss of BMP inhibition disrupts inductive effects of the endothelium that are necessary to differentiate the pulmonary epithelium.

In previous studies, we showed that BMP-4 induces expression of the activin receptor–like kinase 1 (ALK1), which is activated by BMP-9 to induce MGP (Yao et al., 2006). MGP then provides feedback inhibition to BMP through direct protein–protein interactions (Yao et al., 2008) and efficiently regulates BMP-4 activity in both pulmonary epithelium and vascular endothelium (Yao et al., 2011). BMP-4 is an essential early driver of EC differentiation and lung development, and the regulation of BMP-4 activity by MGP is critical for the coordination between the vasculature and airways (Yao et al., 2007). In this study, we examine the time course of MGP expression during derivation of ECs and lung endoderm from ESCs. We find that the induction of MGP occurs in both processes, but to a higher level in the lung endoderm than in the ECs (Fig. 7 f). Thus, we show that loss of MGP has a permissive effect on BMP-4 activity and allows it to induce Flt1 in the endothelium and VEGF and c-Met in the epithelium. VEGF then activates Flt1 to induce HGF, which elicits its effect through c-Met to cause hepatic differentiation in $Mgp^{-/-}$ pulmonary progenitor cells. This emphasizes the balance between BMP-4 and MGP as an agonist and suggests that it is sufficient to remove an antagonist to achieve changes in differentiation. It is also noteworthy that both endothelium and epithelium need to be depleted of MGP to trigger the hepatic differentiation because MGP acts in the extracellular space. Altogether, the results suggest that, in early lung development, MGP regulates BMP-4 activity in cross talk between pulmonary epithelium and vascular endothelium to direct pulmonary specification. We also examined the activity of other BMPs to determine whether our findings were specific for BMP-4. We found that excess BMP-2, -7, and -9 had no effect on the expression of VEGF, Flt1, HGF, and c-Met in pulmonary endothelium, suggesting that the excess BMP-4 activity is driving the hepatic differentiation in $Mgp^{-/-}$ lungs.

Inductive effects of vascular endothelium have been shown to play key roles in developmental processes during organogenesis, including pulmonary and hepatic differentiation (Stainier et al., 1995; Matsumoto et al., 2001; Lee et al., 2014). Because the lungs and liver emerge in close proximity from the foregut endoderm (Herriges and Morrisey, 2014; Miyajima et al., 2014), the local environment, which is composed of extracellular proteins, is critical for specifying the differentiation. ECs release BMPs in response to several stimuli (Sorescu et al., 2003; Csiszar et al., 2006; Boström et al., 2011), and the BMP distribution constitutes a key factor in lung development (Bellusci et al., 1996; Weaver et al., 2000). It is possible that expression of MGP, which begins around the emergence of the lung bud (Gilbert and Rannels, 2004), controls BMP activity in the regulation of endothelial-inductive effects that promote airway progenitor cells and suppress hepatic differentiation.

Although we find that HGF acts as a key factor in the abnormal hepatic differentiation in $Mgp^{-/-}$ lungs, participation of other extracellular factors, BMP-4 in particular, is essential. BMP-4 has been used as an initiating factor in the derivation of hepatocytes from ESCs or hepatic progenitor cells (Gouon-Evans et al., 2006; Fan et al., 2009). The expression of MGP is minimal in liver (Yao et al., 2016), and loss of MGP has no clear effect on the liver (Luo et al., 1997). However, there is evidence that other BMP inhibitors, such as Noggin, are involved in hepatic specification (Matsumoto et al., 2001). Excess Noggin inhibits hepatic differentiation induced by BMP-4 (Matsumoto et al., 2001), suggesting that hepatic Noggin may play a role in the interactions between hepatic endothelium and hepatocytes.

Foxa2 is an important factor for the development of endoderm-derived organs, such as liver, lungs, pancreas, and stomach (Nagy et al., 1994; Kimura et al., 1996; Zhou et al., 1997; Wan et al., 2005; Kaestner, 2010). In adult lungs, Foxa2 is detected in the bronchiolar epithelium and alveolar type II cells (Besnard et al., 2004). It functions as a key factor in alveolarization during lung development (Wan et al., 2005) but is also critical for the hepatic development (Lee et al., 2005; Bochkis et al., 2009). The interaction between Foxa2 and the lung-specific factor Nkx2.1 occurs in the pulmonary epithelium, and their cooperation represses metastasis of pulmonary adenocarcinoma (Snyder et al., 2013; Li et al., 2015). Furthermore, collaboration between Foxa2, Hnf4a, and other factors drives adult fibroblasts and ESCs into hepatocyte-like cells (Sekiya and Suzuki, 2011;

(n = 2). (c) Expression of albumin (Alb), Ttr, Pah, and AFP was determined in lungs by real-time PCR (n = 3). (d) The total amount of albumin (right) and activity of P450 (left) was determined in cells isolated from lungs (n = 8). Data in c and d were analyzed by two-sided t test. ***, $P < 0.001$. Error bars are standard deviation. Data distribution was assumed to be normal, but this was not formally tested.

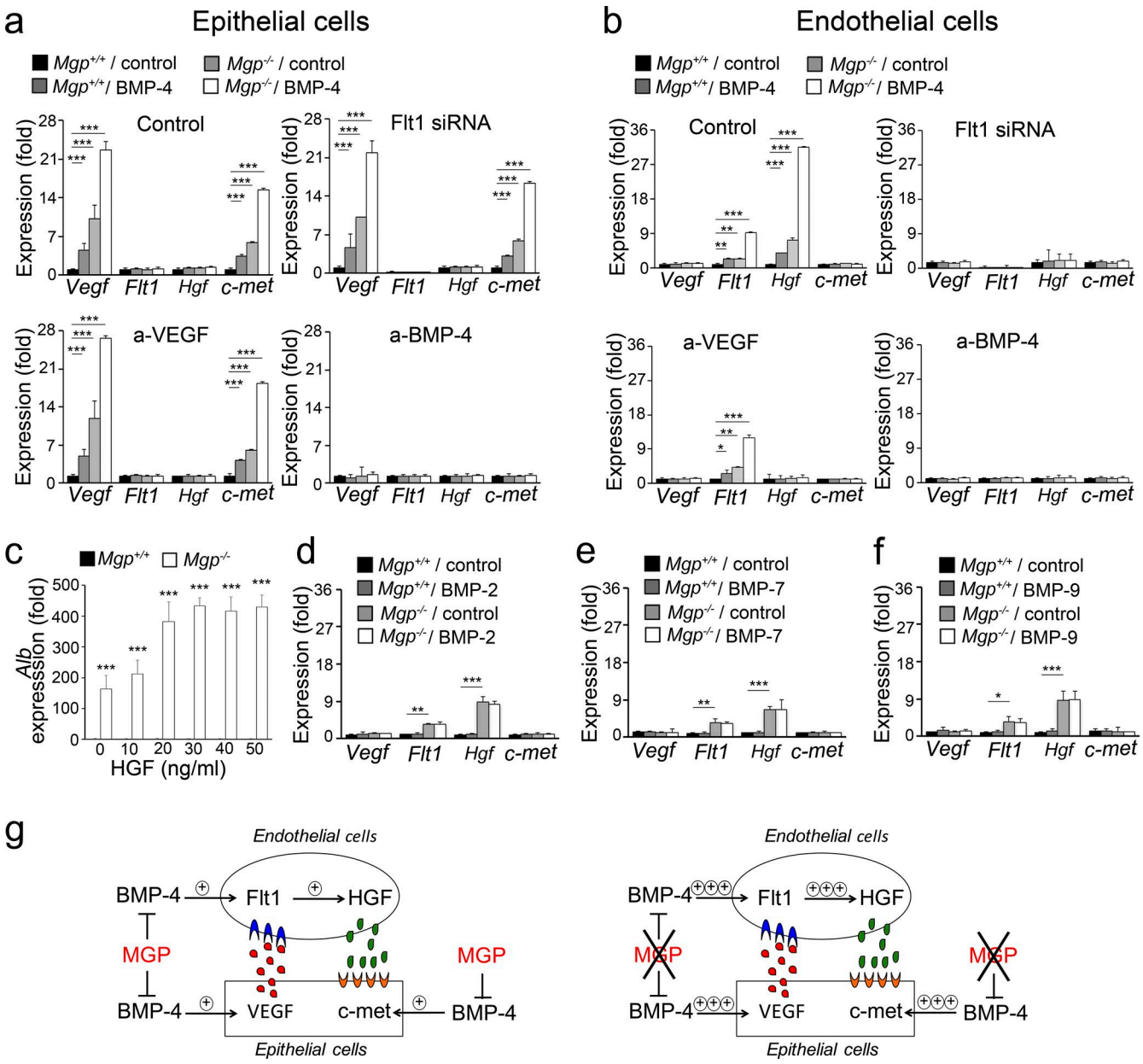

Figure 6. **Cross talk between endothelial and epithelial cells induces HGF in *Mgp*$^{-/-}$ lungs.** (a and b) Epithelial cells (a) and ECs (b) isolated from *Mgp*$^{+/+}$ and *Mgp*$^{-/-}$ lungs were treated with BMP-4, anti-VEGF or anti–BMP-4 (a-BMP-4) antibodies, or transfected with Flt1 siRNA. Expression of VEGF, Flt1, HGF, and c-Met was determined by real-time PCR after 24 h of treatment (n = 3). (c) Expression of albumin (Alb) in epithelial cells was isolated from *Mgp*$^{+/+}$ and *Mgp*$^{-/-}$ lungs and treated with HGF for 24 h (n = 3). (d–f) Expression of VEGF, Flt1, HGF, and c-Met in ECs was isolated from *Mgp*$^{+/+}$ and *Mgp*$^{-/-}$ lungs and individually treated with BMP-2, -7, and -9 (n = 3). (g) Schematic diagram of cross talk between ECs and epithelial cells. Data in a–f were analyzed by two-sided t test. *, P < 0.05; **, P < 0.01; ***, P < 0.001. Error bars are standard deviation. Data distribution was assumed to be normal, but this was not formally tested.

Du et al., 2014). Here, we show that Hnf4a is induced by HGF and binds to Foxa2 in *Mgp*$^{-/-}$ lungs to initiate hepatic differentiation. Thus, Foxa2 and Hnf4a may work together to cause ectopic hepatic differentiation in nonliver organs, and BMP inhibition appears essential for suppression of Hnf4a during pulmonary differentiation. However, the binding of Hnf4a and Foxa2 competes with that of Foxa2 and Nkx2.1 and could affect lung development through this mechanism.

Our observation differs from reported cases of ectopic liver tissues in human lungs (Hudson and Brown, 1962; Lasser and Wilson, 1975; Mendoza et al., 1986; Iber and Rintala, 1999; Chalak and Parham, 2007; Choi et al., 2008; Tancredi et al., 2010; Bannon et al., 2013). In *Mgp*$^{-/-}$ mouse, the lungs still develop and function, although the alveolar structures and pulmonary vasculature are abnormal. In contrast, the reported ectopic liver tissue in the lungs does not resemble pulmonary tissue and may result from translocation of hepatocytes into the lungs because of unknown reasons. Interestingly, peptidomics of bronchoalveolar lavage fluid from premature neonates with bronchopulmonary dysplasia reveal high concentrations of albumin fragments that could not be ascribed to an enhanced diffusion of albumin from serum (Vento et al., 2009). It is possible that it could be an indication of abnormalities involving enhanced BMP signaling.

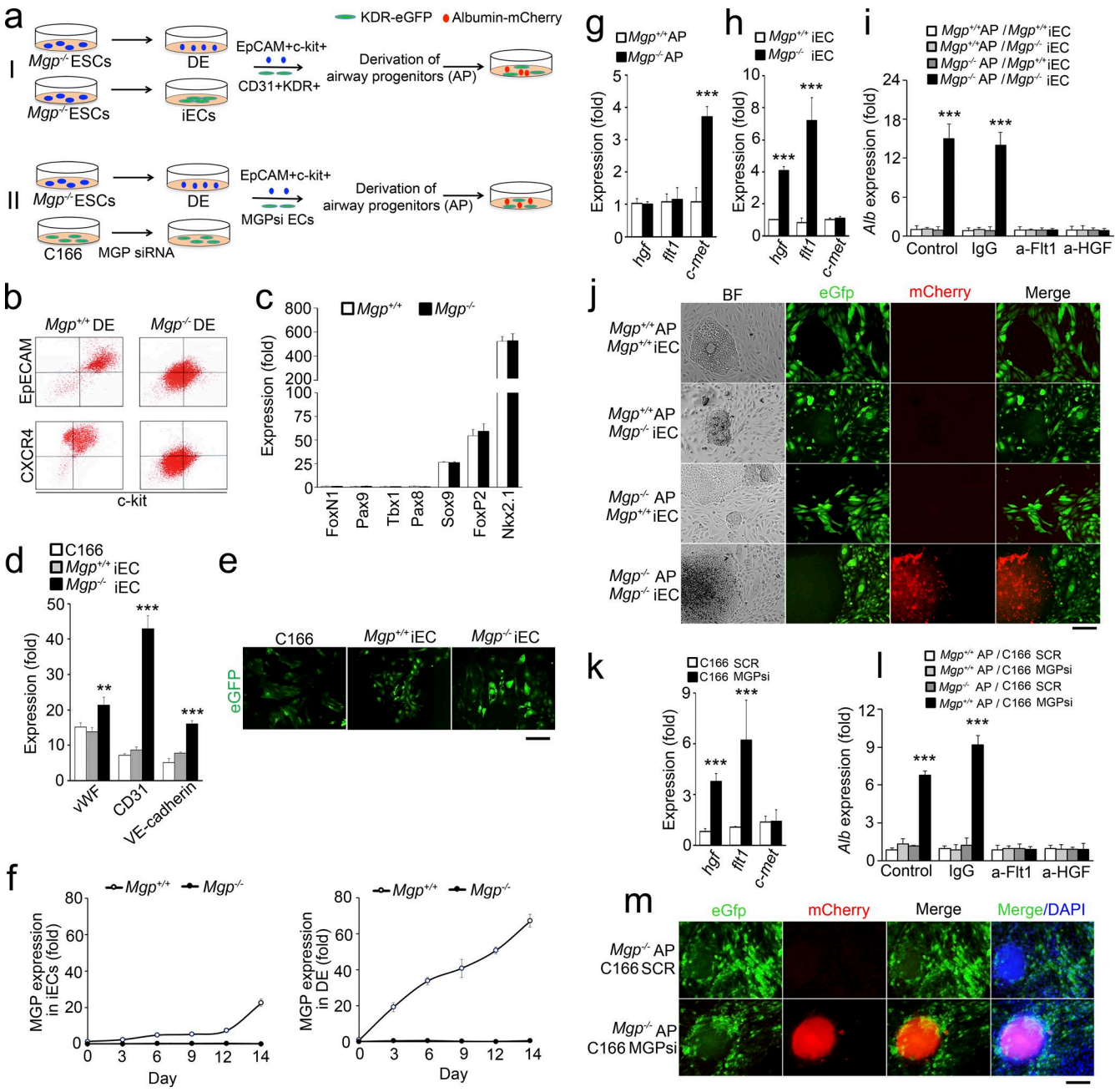

Figure 7. **Albumin induced in airway progenitors derived from *Mgp*$^{-/-}$ ESCs when co-cultured with *Mgp*$^{-/-}$ ECs.** (a) Schematic diagram of the experimental strategy. KDR, kinase insert domain receptor. (b) Flow cytometric analysis of EpCAM^{+}c-kit^{+} and CXCR4^{+}c-kit^{+} cell populations in definitive endoderm (DE) derived from WT (*Mgp*$^{+/+}$) and *Mgp*$^{-/-}$ ESCs (n = 3). (c) Gene expression of lineage markers was determined by real-time PCR with normalization to GAPDH expression in airway progenitors derived from WT (*Mgp*$^{+/+}$) and *Mgp*$^{-/-}$ EpCAM^{+}c-kit^{+} definitive endoderm cells. Fold changes of expression are calculated as compared with the FoxN1 expression in *Mgp*$^{+/+}$EpCAM^{+}c-kit^{+} definitive endoderm cells (n = 3). (d) Expression of von Willebrand factor (vWF), CD31, and VE-cadherin in induced ECs derived from *Mgp*$^{+/+}$ and *Mgp*$^{-/-}$ ESCs. The C166 line is shown as control (n = 3). (e) Expression of EGFP driven by the Flk1 promoter in C166 cells and *Mgp*$^{+/+}$- and *Mgp*$^{-/-}$-induced ECs (n = 5). (f) Time course of MGP expression during the derivation of EC and definitive endoderm from *Mgp*$^{+/+}$ and *Mgp*$^{-/-}$ ESCs (n = 3). (g) Gene expression of HGF, Flt1, and c-Met was determined by real-time PCR in airway progenitors (AP) derived from *Mgp*$^{+/+}$ and *Mgp*$^{-/-}$ EpCAM^{+}c-kit^{+} definitive endoderm cells (n = 3). (h) Gene expression of HGF, Flt1, and c-Met was determined by real-time PCR in induced ECs derived from *Mgp*$^{+/+}$ and *Mgp*$^{-/-}$ ESCs (n = 3). (i) Albumin expression was determined by real-time PCR in Nkx2.1^{+}FoxP2^{+} cells derived from *Mgp*$^{+/+}$ and *Mgp*$^{-/-}$ EpCAM^{+}c-kit^{+} definitive endoderm cells with co-culture of *Mgp*$^{+/+}$ and *Mgp*$^{-/-}$ ECs. Anti-Flt1 (a-Flt1) and anti-HGF (a-HGF) were added to neutralize Flt1 and HGF, respectively (n = 3). (j) EGFP and mCherry were determined in the co-culture of airway progenitors and ECs by fluorescence microscopy (n = 4). BF, bright field. (k) Gene expression of HGF, Flt1, and c-Met was determined by real-time PCR in C166 ECs transfected with scrambled siRNA (SCR) or MGP siRNA (si) (n = 3). (l) Albumin expression was determined by real-time PCR in Nkx2.1^{+}FoxP2^{+} cells derived from *Mgp*$^{+/+}$ and *Mgp*$^{-/-}$ EpCAM^{+}c-kit^{+} definitive endoderm cells with co-culture of MGP-depleted C166 ECs. a-Flt1 and a-VEGF were added to neutralize Flt1 and VEGF, respectively (n = 3). (m) EGFP and mCherry were determined by fluorescence microscopy in airway progenitors derived from *Mgp*$^{-/-}$ EpCAM^{+}c-kit^{+} definitive endoderm cells with co-culture of C166 ECs (n = 5). Data in c and d, f–i, and k and l were analyzed by two-sided t test. **, $P < 0.01$; ***, $P < 0.001$. Error bars are standard deviation. Data distribution was assumed to be normal, but this was not formally tested. Bars, 50 µm.

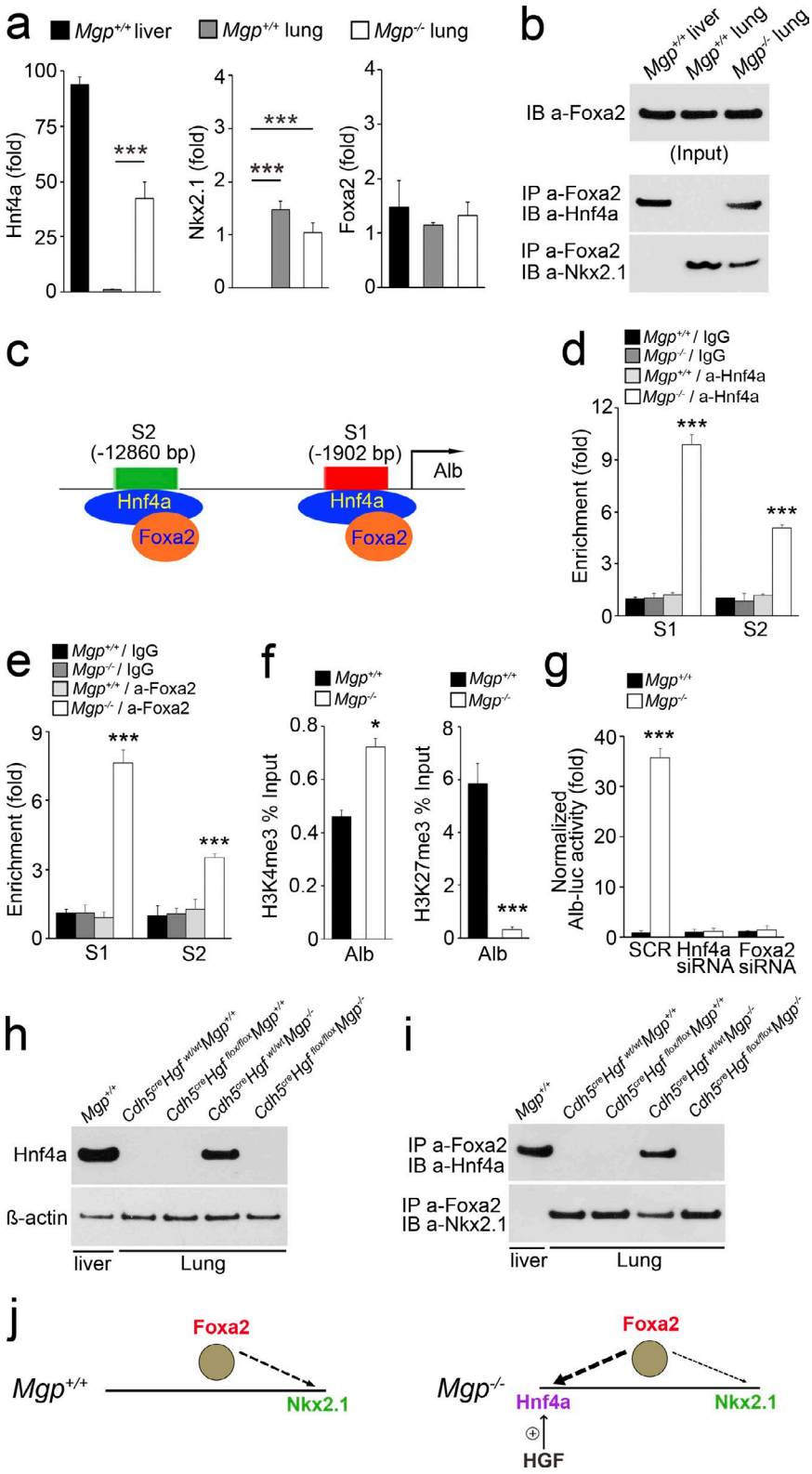

Figure 8. **HGF-induced Hnf4a binds to Foxa2 in *Mgp*$^{-/-}$ lungs.** (a) Expression of Hnf4a, Nkx2.1, and Foxa2 was determined in lungs by real-time PCR (n = 5). Liver of WT mice was used as a control. (b) Protein interactions in lung lysates were analyzed by immunoprecipitation (IP), followed by immunoblotting (IB) with antibodies as indicated (n = 6). Lysates from WT *Mgp*$^{+/+}$ liver were used as a positive control. (c–f) Hnf4a and Foxa2 bind to the albumin locus at the Hnf4a-binding site and alter the albumin transcription state in *Mgp*$^{-/-}$ lungs, as detected by ChIP assays (n = 3). (g) Luciferase assay of pulmonary epithelial cells integrated with luciferase reporter driven by the albumin promoter and transfected with scrambled siRNA (SCR), Hnf4a siRNA, or Foxa2 siRNA (n = 3). (h) Expression of Hnf4a was determined in lungs of *Cdh5*^{Cre}*Hgf*$^{wt/wt}$*Mgp*$^{+/+}$, *Cdh5*^{Cre}*Hgf*$^{flox/flox}$*Mgp*$^{+/+}$, *Cdh5*^{Cre}*Hgf*$^{wt/wt}$*Mgp*$^{-/-}$, and *Cdh5*^{Cre}*Hgf*$^{flox/flox}$*Mgp*$^{-/-}$ mice by immunoblotting. WT *Mgp*$^{+/+}$ liver was used as a control (n = 3). (i) Protein interactions of lung lysates were analyzed by immunoprecipitation, followed by immunoblotting with antibodies as indicated (n = 6). Lysates from WT *Mgp*$^{+/+}$ liver were used as a positive control. (j) Schematic diagram of the binding of Hnf4a and Foxa2 competing with that of Foxa2 and Nkx2.1 in *Mgp*$^{-/-}$ lungs. Data in a and d–g were analyzed by two-sided t test. *, $P < 0.05$; ***, $P < 0.001$. Error bars are standard deviation. Data distribution was assumed to be normal, but this was not formally tested.

Altogether, our results support a critical role for BMP inhibition, as provided by MGP, in epithelial–endothelial interactions between vascular endothelium and pulmonary epithelium to prevent hepatic differentiation from occurring during pulmonary specification.

Materials and methods

Animals

Mgp$^{+/-}$ (B6.129S7-Mgptm1Kry/KbosJ), *Cdh5*^{Cre} (B6.Cg-Tg(Cdh5-cre)7Mlia/J), *Alb*^{Cre} (B6.Cg-Tg(Alb-cre)21Mgn/J), *Rosa*^{LacZ} (B6;

129S4-Gt(ROSA)26Sortm1Sor/J), and *Rosa*^{eGfp} (B6;129-Gt(ROSA)26Sortm2Sho/J) mice on a C57BL/6J background were obtained from the Jackson Laboratory. *Hgf*$^{flox/flox}$ (B6;129-Hgftm1Jmw/Mmnc) mice were obtained from the Mutant Mouse Resource and Research Center. Genotypes were confirmed by PCR (Yao et al., 2012), and experiments were performed with generations F4–F6. Littermates were used as WT controls. All mice were fed a standard chow diet (Diet 8604; HarlanTeklad Laboratory). The studies were reviewed and approved by the Institutional Review Board and conducted in accordance with the animal care guidelines set by the University of California, Los Angeles. The investigation conformed to the standards of the National Research Council (2011).

Maintenance and differentiation of ESCs

E14.1 mouse ESCs (C57BL/6J background) were obtained from the American Type Culture Collection (SCRC-1002) and used as WT ESCs in this study. Before induction of differentiation, ESCs were cultured in Glasgow minimum essential medium (Invitrogen) containing 10% knockout serum replacement (Invitrogen), 1% FBS (HyClone), 1% penicillin/streptomycin/glutamine, 1% nonessential amino acids (Invitrogen), 0.1 mM 2-mercaptoethanol, 1 mM sodium pyruvate, and 1,000 U/ml leukemia inhibitory factor (ESGRO). The medium was changed daily.

The protocol adopted for lung differentiation was performed as previously described (Mou et al., 2012). The ESCs were trypsinized, quenched with FBS, centrifuged, and plated onto gelatin-coated dishes for murine embryonic fibroblast depletion for 30 min. ESCs were subsequently cultured at a density of 5–8 × 10^3 cells/cm^2 in day 0 medium (advanced DMEM with 2% B-27 minus vitamin, 0.05% Albumax II, Glutamax, and Y-27632). On day 2, the cells were placed with day 2 differentiation medium (advanced DMEM with 2% FBS, Glutamax, 5 nM GSK3iXV, and 50 ng/ml activin A; 338-AC; R&D Systems). On day 3, the cells were fed with day 2 medium, 50 ng/ml activin A, and 5 M dorsomorphin (P5499; Sigma-Aldrich). To anteriorize endoderm, on and after day 5, the cells were split and fed with day 0 medium and 0.5–1 mM A8301 (616454; CalBiochem) for 2 d. Then, the cells were rinsed with day 0 medium two times and switched to day 0 medium supplemented with 50 ng/ml BMP-4, 100 ng/ml FGF-2 (PHG0026; GIBCO), and 5–10 nM GSK3iXV for another 2–3 d. To generate Nkx-2.1$^+$Sox2$^+$ proximal progenitor cells, the cells were rinsed with day 0 medium two times and switched to day 0 medium containing retinoic acid–supplemented B-27, 50 ng/ml BMP-7, 50 ng/ml FGF-7, 100 nM IWR-1, and 1–2 mM PD98059 for 2 d or longer.

EC differentiation was performed as previously described (Israely et al., 2014). The differentiation of ESCs was performed in serum-free media (StemPro-34; Invitrogen), reconstituted according to the manufacturer's instructions, and supplemented with 1× L-glutamine, 1× β-mercaptoethanol, 0.5 mM ascorbic acid (Millipore), and 200 µg/ml bovine holotransferrin (Sigma-Aldrich). Differentiation of ESCs was performed in 10-cm nontissue culture-treated Petri dishes for 14 d, followed by adherent culture on gelatin-coated 6-well plates in a humidified incubator at 37°C with 5% CO_2. On day 1, 5 ng/ml BMP-4 was added. On day 2, the media were supplemented with 5 ng/ml of fresh BMP-4, 5 ng/ml activin A, and 10 ng/ml FGF-2. On day 3, the media were supplemented with 5 ng/ml of fresh BMP-4, 10 ng/ml FGF-2, and 20 ng/ml VEGF-A. On day 5, the media were supplemented by adding 10 ng/ml of fresh FGF-2 and 20 ng/ml VEGF-A. The media were then refreshed every 2 d with 5 ng/ml FGF-2 and 5 ng/ml VEGF-A.

For co-culture, the day 7 anteriorized definitive endoderm cells from both WT and *Mgp* knockout ESCs were dissociated, and the EpCAM$^+$c-kit$^+$ cells were isolated by FACS and subsequently plated on gelatin-coated dishes in Nkx2.1 induction media. The co-culture endothelial partner cells included CD31$^+$KDR$^+$cells sorted on day 7 of endothelial differentiation in ESCs, mouse yolk sac EC C166 (CRL-2581; American Type Culture Collection) with or without MGP expression, and adult mouse lung ECs with or without MGP sorted by EGFP from *Cdh5-EGFP-Mgp*$^{+/+}$ and *Cdh5-EGFP-Mgp*$^{-/-}$ mice. The EpCAM$^+$c-kit$^+$ cells were co-cultured with EC counterparts at a ratio of 1:1, i.e., 50,000:50,000 cells per well of a 48-well plate. Inhibition of Flt1 and HGF was performed by adding 2 µg/ml Flt1- or HGP-neutralizing antibodies (R&D Systems) every other day starting on day 7. 1 µg/ml of the isotype IgG or 5 mM DMSO (Sigma-Aldrich) was added to the media as controls.

Expression profiles

Total mRNA was extracted from aortic tissues and examined by the MouseRef-8 v2.0 BeadChip kit (Illumina). The array data were analyzed using GenomeStudio software (Illumina). The expression profiles were extracted from array data, and the heat map was generated using GenomeStudio.

RNA analysis

Total RNA was extracted from cells and tissues using the RNeasy mini or micro kit (Qiagen). cDNA was produced by using the high-capacity cDNA reverse transcription kit (Applied Biosystems) according to the manufacturer's instructions. Relative quantitative PCR was performed on a 7500 Fast Real-Time PCR System (Applied Biosystems) using TaqMan Universal PCR Master Mix (Applied Biosystems). Cycle conditions were one cycle at 50°C for 2 min, one cycle at 95°C for 10 min, and then 40 cycles at 95°C for 15 s and 60°C for 1 min. Threshold cycles of specific cDNAs were normalized to the housekeeping gene *GAPDH* and translated to relative values. The TaqMan for mouse albumin (Mm00802090_m1), Ttr (Mm00443266_m1), Pah (Mm00500918_m1), GATA4 (Mm00484689_m1), Foxa3 (Mm00484714_m1), Hnf1a (Mm00493434_m1), Hnf4a (Mm01247712_m1), AFP (Mm00431715_m1), Hex (Mm00599877_m1), HGF (Mm01135184_m1), Apof (Mm00506066_g1), Apod (Mm01342307_m1), Apoe (Mm01307193_g1), Apoc1 (Mm00431816_m1), Apoa1 (Mm00437569_m1), Apom (Mm00444525_m1), Apoh (Mm00496516_m1), Apoa2 (Mm00442687_m1), Apoc4 (Mm00545713_m1), Apoc3 (Mm00445670_m1), Apoa5 (Mm00475480_m1), Apoa4 (Mm00431814_m1), Nkx2.1 (Mm01702813_m1), Flt1 (Mm00438980_m1), FoxN1 (Mm00433948_m1), Pax9 (Mm00440629_m1), Tbx1 (Mm00448949_m1), Pax8 (Mm00440623_m1), Sox9 (Mm00448840_m1), FoxP2 (Mm00475030_m1), c-Met (Mm01156972_m1), VEGF (Mm00437306_m1), Aqp5 (Mm00437578_m1), CCSP (Mm00442046_m1), Spd (Mm00445061_m1), Spc (Mm00488144_m1), Spb (Mm00455678_m1), Flk1 (Mm01222421_m1), VE-cadherin (Mm00486938_m1), CD31 (Mm01242576_m1), and Foxa2 (Mm01976556_s1) was obtained from Applied Biosystems as part of TaqMan gene expression assays.

Immunofluorescence

Tissue sections were fixed in 4% paraformaldehyde and processed as previously described (Yao et al., 2016). For immunohistochemistry or immunofluorescence, sections were permeabilized with 0.5% Triton X-100 for 10 min, followed by three washes with wash buffer (WB; PBS containing 0.1% Tween 20). Nonspecific antibody-binding sites were blocked by incubating the sections for 30 min in blocking buffer (1% BSA, 2% goat serum, and 0.5% Triton X-100 in PBS). Primary antibodies were diluted in antibody buffer (1% BSA and 0.5% Triton X-100) in PBS, and sections were incubated for 60 min at room temperature, followed by several washes in WB. Alexa Fluor (AF) 488–conjugated (green fluorescence) or AF594-conjugated (red fluorescence) secondary anti–goat or anti–rabbit antibodies (Molecu-

lar Probes) were applied to the sections and incubated for 30 min at room temperature. After several washes in WB and a brief equilibration of the sections with PBS, the nuclei were stained with DAPI (Sigma-Aldrich). A DAPI stock solution was diluted to 300 nM in PBS, and 300 µl of the diluted solution was added to the sections, making certain that they were completely covered. The samples were incubated for 1–5 min and rinsed several times in PBS. Staining without primary antibodies served as controls. We used specific antibodies for Sox9 (mouse ab76997; Abcam), Foxp2 (rabbit ab16046; Abcam), albumin (goat A90-134A; Bethyl), Aqp5 (rabbit 178615; Millipore), Spb (mouse ab3282; Abcam), CCSP (rabbit 07–623; Millipore), Nkx2.1 (rabbit ab40874; Abcam), MGP (rabbit ab86233; Abcam), HGF (goat AF2207; R&D Systems), and CD34 (rat 551387; BD Biosciences).

Flow cytometric analysis

The cells were detached from the culture dish with 0.25% trypsin/EDTA, centrifuged at low speed, and stained with FITC-, phycoerythrin (PE)-, or AF488-conjugated antibodies. Nonspecific fluorochrome- and isotype-matched IgGs (BD PharMingen) served as controls. Flow cytometer gates were set using unstained cells and the isotype-matched controls. Cells were gated by forward scatter versus side scatter to eliminate debris. A region was established to define positive PE/AF488 fluorescence using a PE/AF488-conjugated, isotype-specific control. The number of cells stained positive for a given marker was determined by the percentage of cells present within a gate, which was established such that <2% of positive events represented nonspecific binding by the PE/AF488-conjugated, isotype-specific control. Minimums of 10,000 events were counted for each analysis. All FACS analyses were performed using a flow cytometer (LSR II; BD Biosciences). FACS files were exported and analyzed using Cellquest software v.3.3 (BD). The cells were stained with antibodies against albumin (goat A90-134A; Bethyl), AFP (mouse 7741; Cell Signaling), EPCAM (rat 552370; Becton, Dickinson and Company), CXCR4 (rabbit ab2074; Abcam), and c-kit (BD Biosciences).

Immunoblotting and immunoprecipitation

For immunoprecipitation, anti–mouse Foxa2 antibodies (rabbit ab76013; Abcam) were cross-linked to Dynabeads protein G (Thermo Fisher). 40 µl Dynabeads was incubated with Foxa2 antibodies for 1 h before washing and incubation with cell extract. Dynabead–antibody complexes were later added to lung extracts from WT and *Mgp*$^{-/-}$ mice (300 µg of protein per sample) with gentle rotation at 4°C for 4 h. Beads were subsequently washed three times with 10 mM Tris-HCl, pH 7.5, and 50 mM KCl. Elution was performed by heating the beads for 10 min at 70°C in 20 µl NuPage loading buffer (Invitrogen) containing 100 mM DTT or SDS elution buffer (2% SDS, 100 mM Tris-HCl, pH 7.5, 10% glycerol, 0.5 mM EDTA, 100 mM DTT, and bromophenol blue as tracer). After removal of the supernatant, the procedure was repeated, and the combined supernatants were neutralized with 2 µl of 1 M Tris, pH 10.0. The eluates were analyzed by immunoblotting. For immunoblotting, equal amounts of tissue lysates were used. Blots were incubated with specific antibodies to Foxa2 (rabbit ab76013; Abcam), Hnf4a (mouse ab41898; Abcam), and Nkx2.1 (rabbit ab40874; Abcam). β-Actin (mouse a2228; Sigma-Aldrich) was used as a loading control.

ELISA

The level of albumin was examined by using an ELISA kit (Abcam). The assays were performed in accordance with the manufacturer's protocols.

P450 activity

The activity of P450 was measured by a cytochrome P450 reductase activity assay kit (Abcam). Equal amounts of tissue lysates were measured. The assays were performed in accordance with the manufacturer's protocols.

ChIP assay

For each ChIP assay, ∼10^6 cells were cross-linked in 1% formaldehyde for 10 min at room temperature. Glycine was added to a concentration of 0.125 M to quench the cross-linking. The cells were then rinsed with ice-cold PBS, resuspended and lysed in lysis buffers, and sonicated to shear the cross-linked DNA to fragments ranging from 200 to 500 bp as previously described by Collas (2010). Sonication was performed on a 4000 Sonicator (Misonix) while the samples were kept immersed in an ice water bath, and 1/10–1/20 of the sonicated lysate was saved for input DNA extraction. The lysate was incubated with 1 µg anti–mouse Hnf4a (mouse ab41898; Abcam), anti–mouse Foxa2 (rabbit ab76013; Abcam), anti-H3K4me3 (rabbit ab8580; Abcam), and anti-H3K27me3 (mouse ab6002; Abcam) antibodies or normal IgG at 4°C overnight. After adding 40 µl protein G magnetic beads, the lysate was further incubated for 2–3 h. The beads were washed repeatedly, and DNA was eluted from the beads by incubating in 10 mM Tris-Cl, pH 8.5, for 15 min at 65°C. Both the immunoprecipitated and input DNA samples were incubated overnight at 65°C for reversal of cross-linking. The DNA samples were then purified by sequential phenol/chloroform/isoamyl alcohol (Sigma-Aldrich). The final DNA products were ethanol precipitated, and the pellets were air dried and dissolved in 10 mM Tris-HCl. The following primers were used for the ChIP assay: Hnf4a site 1 was forward, 5′-CCACACTCTCTTCTCCTTCAACC-3′, and reverse, 5′-ATCTCCATTCTACCCTCCCAGTC-3′. Hnf4a site 2 was forward, 5′-TGCATTTGCCAGAAAGTGAAGA-3′, and reverse, 5′-AACCAGCCTCTAATTCCCGTGT-3′. H3K4me3 and H3K27me3 were forward, 5′-TTTAACTCCCCGTAACTCATGT-3′, and reverse, 5′-GGCAGTGATGGTTGCACAAG-3′.

Pulmonary function test

Mice were weighed and placed into a single chamber with a volume of 0.8 liters, where they were allowed to move freely and acclimate for at least 15 min. To provide a baseline reading, a room air reading was taken as follows: compressed air was supplied to the chamber at a flow rate of 1 liter/min for 45 min. At this point, the chamber was completely sealed, with airflow momentarily stopped. The changes in pressure caused by breathing were recorded and amplified by Fine Pointe. Subsequently, the mice were allowed to rest for at least 5 min or until the breathing returned to baseline before conducting the hypercapnia phase. In the hypercapnia phase, a gas mixture containing 7% CO_2, 21% O_2, and balanced N_2 was supplied to the chamber at a flow of 1 liter/min. After 5 min, the chamber was sealed, and ventilatory patterns were recorded. During the room air breathing and hypercapnia phase, the mean tidal volume and respiratory rate were measured for a period of at least 10 consecutive breaths. To avoid an excessive build-up in CO_2 concentration within the chamber caused by rebreathing, a Bias flow regulator (Buxco Electronics, Inc.) was used. The Bias flow regulator provided a quiet, constant, and smooth flow through the animal chamber that prevented CO_2 build-up. The following parameters were recorded: respiratory rate, tidal volume, peak inspiration flow, peak expiratory flow, and minute ventilation, which was calculated and corrected for body weight. The mean values were calculated once per minute for each serial 10 min. The machine was sanitized with alcohol between uses.

Luciferase assay and siRNA transfection

For luciferase assays, the cells were lysed in 100 µl Passive Lysis Buffer (Promega) per well in 24-well plates. The cells were freeze-thawed twice and agitated for 15 min. Two 20-µl aliquots from each

well were used for luciferase assays (Promega). Luciferase activity was determined using a luminometer (AutoLumat LB953; PerkinElmer Life Sciences) and expressed as mean ± standard deviation from quadruplicate experiments. The construction, in which luciferase was driven by albumin promoter, was obtained from GeneCopoeia (MPRM26381-PG02). Transient transfections with siRNA were performed with Lipofectamine 2000 (Invitrogen) using 60 nM siRNA. siRNAs to Hnf4a (s67635; sense: 5′-AGAGGUCCAUGG UGUUUAATT-3′; antisense: 5′-UUAAACACCAUGGACCUC UTG-3′; Thermo Fisher) and Foxa2 (s67629; sense: 5′-GAGGGC UACUCUUCCGUGATT-3′; antisense: 5′-UCACGGAAGAGUAGC CCUCGG-3′; Thermo Fisher) were used for experiments. Scrambled siRNA was used as a control.

Fluorescence microscopy

Images were captured by a microscope (Eclipse Ti-s; Nikon) with digital camera (DS-Fi2; Nikon) at room temperature. Three different magnification objective lenses (4×, 10×, and 20×) were used, and the acquisition software was NIS Elements Br. AF488-conjugated (green fluorescence) or AF594-conjugated (red fluorescence) secondary antibodies (Molecular Probes) were applied to the sections. EGFP or mCherry was used as tagged markers for molecules in live cells. All images of live cells were captured in DMEM.

Statistical analysis

A two-sided *t* test was used to analyze the data. The analyses were performed using Instat version 3.0 (GraphPad Software). Data represent mean ± standard deviation. P-values <0.05 were considered significant, and experiments were repeated a minimum of three times. Data were analyzed for statistical significance by ANOVA with post-hoc Tukey's analysis.

Online supplemental material

In the online supplemental material, we showed the expression of apolipoproteins in $Mgp^{+/+}$ and $Mgp^{-/-}$ lungs and examined $Mgp^{+/+}$ and $Mgp^{-/-}$ lungs by using transmission EM (Fig. S1). We showed expression of pulmonary markers in the lungs and livers of $Mgp^{+/+}$, $Mgp^{-/-}$, and $Mgp^{tg/wt}$ and $Mgp^{-/-}$mice (Fig. S2). We examined the expression of EGFP in the lungs of $Alb^{Cre}Rosa^{EGFP}Mgp^{-/-}$ mice and verified that Hnf4a binds to the *Ttr* gene promoter, but not the Pax8 promoter in $Mgp^{-/-}$ lungs, by using ChIP assays (Fig. S3 and Fig. S4).

Acknowledgments

Funding for this work was provided in part by National Institutes of Health grants NS79353, HL30568, HL81397, and HL112839 and the American Heart Association (Western Affiliate). The pulmonary function test was performed by the Center for Duchenne Muscular Dystrophy Muscle Phenotyping and Imaging Core, which was partially supported by a grant from the National Institutes of Health (NIH-P30-5P30AR057230; Spencer-PI).

The authors declare no competing financial interests.

Author contributions: Y. Yao and K.I. Boström supervised the experiments, analyzed data, and wrote the manuscript. J. Yao, X. Wu, P.J. Guihard, A.M. Blazquez-Medela, M.J. Spencer, M. Jumabay, P. Tontonoz, and A.M. Fogelman performed experiments and/or data analysis.

Submitted: 16 December 2016
Revised: 26 April 2017
Accepted: 12 July 2017

References

Alva, J.A., A.C. Zovein, A. Monvoisin, T. Murphy, A. Salazar, N.L. Harvey, P. Carmeliet, and M.L. Iruela-Arispe. 2006. VE-Cadherin-Cre-recombinase transgenic mouse: a tool for lineage analysis and gene deletion in endothelial cells. *Dev. Dyn.* 235:759–767. http://dx.doi.org/10.1002/dvdy.20643

Ballarín-González, B., L.B. Lassen, R. Jessen, A. Füchtbauer, E.M. Füchtbauer, and F.S. Pedersen. 2013. Deregulated Nras expression in knock-in animals harboring a gammaretroviral long terminal repeat at the Nras/Csde1 locus. *PLoS One.* 8:e56029. http://dx.doi.org/10.1371/journal.pone.0056029

Bannon, K., J. Hraemic, and V. Mittal. 2013. Ectopic liver tissue sequestered in the lung. *Am. Surg.* 79:E104–E105.

Bellusci, S., R. Henderson, G. Winnier, T. Oikawa, and B.L. Hogan. 1996. Evidence from normal expression and targeted misexpression that bone morphogenetic protein (Bmp-4) plays a role in mouse embryonic lung morphogenesis. *Development.* 122:1693–1702.

Besnard, V., S.E. Wert, W.M. Hull, and J.A. Whitsett. 2004. Immunohistochemical localization of Foxa1 and Foxa2 in mouse embryos and adult tissues. *Gene Expr. Patterns.* 5:193–208. http://dx.doi.org/10.1016/j.modgep.2004.08.006

Bochkis, I.M., J. Schug, N.E. Rubins, A.R. Chopra, B.W. O'Malley, and K.H. Kaestner. 2009. Foxa2-dependent hepatic gene regulatory networks depend on physiological state. *Physiol. Genomics.* 38:186–195. http://dx.doi.org/10.1152/physiolgenomics.90376.2008

Boström, K.I., M. Jumabay, A. Matveyenko, S.B. Nicholas, and Y. Yao. 2011. Activation of vascular bone morphogenetic protein signaling in diabetes mellitus. *Circ. Res.* 108:446–457. http://dx.doi.org/10.1161/CIRCRESAHA.110.236596

Chalak, L.F., and D.M. Parham. 2007. A newborn with Poland anomaly and liver ectopy: an unusual association with important prognostic implications. *Pediatr. Dev. Pathol.* 10:134–137. http://dx.doi.org/10.2350/06-04-00801.1

Chen, Y., N. Kobayashi, S. Suzuki, A. Soto-Gutierrez, J.D. Rivas-Carrillo, K. Tanaka, N. Navarro-Alvarez, T. Fukazawa, M. Narushima, A. Miki, et al. 2005. Transplantation of human hepatocytes cultured with deleted variant of hepatocyte growth factor prolongs the survival of mice with acute liver failure. *Transplantation.* 79:1378–1385. http://dx.doi.org/10.1097/01.TP.0000160813.37515.97

Choi, S.U., H.K. Kim, and J. Kim. 2008. Heterotopic supradiaphragmatic liver combined with intralobar pulmonary sequestration. *Ann. Thorac. Surg.* 85:1809–1810. http://dx.doi.org/10.1016/j.athoracsur.2007.11.040

Collas, P. 2010. The current state of chromatin immunoprecipitation. *Mol. Biotechnol.* 45:87–100. http://dx.doi.org/10.1007/s12033-009-9239-8

Csiszar, A., M. Ahmad, K.E. Smith, N. Labinskyy, Q. Gao, G. Kaley, J.G. Edwards, M.S. Wolin, and Z. Ungvari. 2006. Bone morphogenetic protein-2 induces proinflammatory endothelial phenotype. *Am. J. Pathol.* 168:629–638. http://dx.doi.org/10.2353/ajpath.2006.050284

Ding, B.S., D.J. Nolan, J.M. Butler, D. James, A.O. Babazadeh, Z. Rosenwaks, V. Mittal, H. Kobayashi, K. Shido, D. Lyden, et al. 2010. Inductive angiocrine signals from sinusoidal endothelium are required for liver regeneration. *Nature.* 468:310–315. http://dx.doi.org/10.1038/nature09493

Ding, B.S., D.J. Nolan, P. Guo, A.O. Babazadeh, Z. Cao, Z. Rosenwaks, R.G. Crystal, M. Simons, T.N. Sato, S. Worgall, et al. 2011. Endothelial-derived angiocrine signals induce and sustain regenerative lung alveolarization. *Cell.* 147:539–553. http://dx.doi.org/10.1016/j.cell.2011.10.003

Du, Y., J. Wang, J. Jia, N. Song, C. Xiang, J. Xu, Z. Hou, X. Su, B. Liu, T. Jiang, et al. 2014. Human hepatocytes with drug metabolic function induced from fibroblasts by lineage reprogramming. *Cell Stem Cell.* 14:394–403. http://dx.doi.org/10.1016/j.stem.2014.01.008

Fan, J., H. Shen, Q. Dai, G.Y. Minuk, F.J. Burzynski, and Y. Gong. 2009. Bone morphogenetic protein-4 induced rat hepatic progenitor cell (WB-F344 cell) differentiation toward hepatocyte lineage. *J. Cell. Physiol.* 220:72–81. http://dx.doi.org/10.1002/jcp.21731

Gilbert, K.A., and S.R. Rannels. 2004. Matrix GLA protein modulates branching morphogenesis in fetal rat lung. *Am. J. Physiol. Lung Cell. Mol. Physiol.* 286:L1179–L1187. http://dx.doi.org/10.1152/ajplung.00188.2003

Gouon-Evans, V., L. Boussemart, P. Gadue, D. Nierhoff, C.I. Koehler, A. Kubo, D.A. Shafritz, and G. Keller. 2006. BMP-4 is required for hepatic specification of mouse embryonic stem cell-derived definitive endoderm. *Nat. Biotechnol.* 24:1402–1411. http://dx.doi.org/10.1038/nbt1258

Hasuike, S., A. Ido, H. Uto, A. Moriuchi, Y. Tahara, M. Numata, K. Nagata, T. Hori, K. Hayashi, and H. Tsubouchi. 2005. Hepatocyte growth factor accelerates the proliferation of hepatic oval cells and possibly promotes the differentiation in a 2-acetylaminofluorene/partial hepatectomy model

in rats. *J. Gastroenterol. Hepatol.* 20:1753–1761. http://dx.doi.org/10.1111/j.1440-1746.2005.03922.x

Herriges, M., and E.E. Morrisey. 2014. Lung development: orchestrating the generation and regeneration of a complex organ. *Development.* 141:502–513. http://dx.doi.org/10.1242/dev.098186

Hudson, T.R., and H.N. Brown. 1962. Ectopic (supradiaphragmatic) liver. *J. Thorac. Cardiovasc. Surg.* 43:552–555.

Iber, T., and R. Rintala. 1999. Intrapulmonary ectopic liver. *J. Pediatr. Surg.* 34:1425–1426. http://dx.doi.org/10.1016/S0022-3468(99)90028-3

Israely, E., M. Ginsberg, D. Nolan, B.S. Ding, D. James, O. Elemento, S. Rafii, and S.Y. Rabbany. 2014. Akt suppression of TGFβ signaling contributes to the maintenance of vascular identity in embryonic stem cell-derived endothelial cells. *Stem Cells.* 32:177–190. http://dx.doi.org/10.1002/stem.1521

Kaestner, K.H. 2010. The FoxA factors in organogenesis and differentiation. *Curr. Opin. Genet. Dev.* 20:527–532. http://dx.doi.org/10.1016/j.gde.2010.06.005

Kimura, S., Y. Hara, T. Pineau, P. Fernandez-Salguero, C.H. Fox, J.M. Ward, and F.J. Gonzalez. 1996. The T/ebp null mouse: thyroid-specific enhancer-binding protein is essential for the organogenesis of the thyroid, lung, ventral forebrain, and pituitary. *Genes Dev.* 10:60–69. http://dx.doi.org/10.1101/gad.10.1.60

Kusumbe, A.P., S.K. Ramasamy, and R.H. Adams. 2014. Coupling of angiogenesis and osteogenesis by a specific vessel subtype in bone. *Nature.* 507:323–328. http://dx.doi.org/10.1038/nature13145

Lasser, A., and G.L. Wilson. 1975. Ectopic liver tissue mass in the thoracic cavity. *Cancer.* 36:1823–1826. http://dx.doi.org/10.1002/1097-0142(197511)36:5<1823::AID-CNCR2820360537>3.0.CO;2-G

Lee, C.S., J.R. Friedman, J.T. Fulmer, and K.H. Kaestner. 2005. The initiation of liver development is dependent on Foxa transcription factors. *Nature.* 435:944–947. http://dx.doi.org/10.1038/nature03649

Lee, J.-H., D.H. Bhang, A. Beede, T.L. Huang, B.R. Stripp, K.D. Bloch, A.J. Wagers, Y.-H. Tseng, S. Ryeom, and C.F. Kim. 2014. Lung stem cell differentiation in mice directed by endothelial cells via a BMP4-NFATc1-thrombospondin-1 axis. *Cell.* 156:440–455. http://dx.doi.org/10.1016/j.cell.2013.12.039

Li, C.M., V. Gocheva, M.J. Oudin, A. Bhutkar, S.Y. Wang, S.R. Date, S.R. Ng, C.A. Whittaker, R.T. Bronson, E.L. Snyder, et al. 2015. Foxa2 and Cdx2 cooperate with Nkx2-1 to inhibit lung adenocarcinoma metastasis. *Genes Dev.* 29:1850–1862. http://dx.doi.org/10.1101/gad.267393.115

Luo, G., P. Ducy, M.D. McKee, G.J. Pinero, E. Loyer, R.R. Behringer, and G. Karsenty. 1997. Spontaneous calcification of arteries and cartilage in mice lacking matrix GLA protein. *Nature.* 386:78–81. http://dx.doi.org/10.1038/386078a0

Matsumoto, K., H. Yoshitomi, J. Rossant, and K.S. Zaret. 2001. Liver organogenesis promoted by endothelial cells prior to vascular function. *Science.* 294:559–563. http://dx.doi.org/10.1126/science.1063889

Meier, M., L.P. Weng, E. Alexandrakis, J. Rüschoff, and G. Goeckenjan. 2001. Tracheobronchial stenosis in Keutel syndrome. *Eur. Respir. J.* 17:566–569. http://dx.doi.org/10.1183/09031936.01.17305660

Mendoza, A., J. Voland, P. Wolf, and K. Benirschke. 1986. Supradiaphragmatic liver in the lung. *Arch. Pathol. Lab. Med.* 110:1085–1086.

Miyajima, A., M. Tanaka, and T. Itoh. 2014. Stem/progenitor cells in liver development, homeostasis, regeneration, and reprogramming. *Cell Stem Cell.* 14:561–574. http://dx.doi.org/10.1016/j.stem.2014.04.010

Mou, H., R. Zhao, R. Sherwood, T. Ahfeldt, A. Lapey, J. Wain, L. Sicilian, K. Izvolsky, K. Musunuru, C. Cowan, and J. Rajagopal. 2012. Generation of multipotent lung and airway progenitors from mouse ESCs and patient-specific cystic fibrosis iPSCs. *Cell Stem Cell.* 10:385–397. http://dx.doi.org/10.1016/j.stem.2012.01.018

Nagy, P., H.C. Bisgaard, and S.S. Thorgeirsson. 1994. Expression of hepatic transcription factors during liver development and oval cell differentiation. *J. Cell Biol.* 126:223–233. http://dx.doi.org/10.1083/jcb.126.1.223

National Research Council. 2011. Guide for the Care and Use of Laboratory Animals. Eighth edition. National Academies Press, Washington, DC.

Odom, D.T., N. Zizlsperger, D.B. Gordon, G.W. Bell, N.J. Rinaldi, H.L. Murray, T.L. Volkert, J. Schreiber, P.A. Rolfe, D.K. Gifford, et al. 2004. Control of pancreas and liver gene expression by HNF transcription factors. *Science.* 303:1378–1381. http://dx.doi.org/10.1126/science.1089769

Postic, C., M. Shiota, K.D. Niswender, T.L. Jetton, Y. Chen, J.M. Moates, K.D. Shelton, J. Lindner, A.D. Cherrington, and M.A. Magnuson. 1999. Dual roles for glucokinase in glucose homeostasis as determined by liver and pancreatic β cell-specific gene knock-outs using Cre recombinase. *J. Biol. Chem.* 274:305–315. http://dx.doi.org/10.1074/jbc.274.1.305

Schmidt, C., F. Bladt, S. Goedecke, V. Brinkmann, W. Zschiesche, M. Sharpe, E. Gherardi, and C. Birchmeier. 1995. Scatter factor/hepatocyte growth factor is essential for liver development. *Nature.* 373:699–702. http://dx.doi.org/10.1038/373699a0

Sekiya, S., and A. Suzuki. 2011. Direct conversion of mouse fibroblasts to hepatocyte-like cells by defined factors. *Nature.* 475:390–393. http://dx.doi.org/10.1038/nature10263

Snyder, E.L., H. Watanabe, M. Magendantz, S. Hoersch, T.A. Chen, D.G. Wang, D. Crowley, C.A. Whittaker, M. Meyerson, S. Kimura, and T. Jacks. 2013. Nkx2-1 represses a latent gastric differentiation program in lung adenocarcinoma. *Mol. Cell.* 50:185–199. http://dx.doi.org/10.1016/j.molcel.2013.02.018

Sorescu, G.P., M. Sykes, D. Weiss, M.O. Platt, A. Saha, J. Hwang, N. Boyd, Y.C. Boo, J.D. Vega, W.R. Taylor, and H. Jo. 2003. Bone morphogenic protein 4 produced in endothelial cells by oscillatory shear stress stimulates an inflammatory response. *J. Biol. Chem.* 278:31128–31135. http://dx.doi.org/10.1074/jbc.M300703200

Soriano, P. 1999. Generalized lacZ expression with the ROSA26 Cre reporter strain. *Nat. Genet.* 21:70–71. http://dx.doi.org/10.1038/5007

Speer, M.Y., H.Y. Yang, T. Brabb, E. Leaf, A. Look, W.L. Lin, A. Frutkin, D. Dichek, and C.M. Giachelli. 2009. Smooth muscle cells give rise to osteochondrogenic precursors and chondrocytes in calcifying arteries. *Circ. Res.* 104:733–741. http://dx.doi.org/10.1161/CIRCRESAHA.108.183053

Stainier, D.Y., B.M. Weinstein, H.W. Detrich III, L.I. Zon, and M.C. Fishman. 1995. Cloche, an early acting zebrafish gene, is required by both the endothelial and hematopoietic lineages. *Development.* 121:3141–3150.

Tancredi, A., A. Cuttitta, D.G. de Martino, and R. Scaramuzzi. 2010. Ectopic hepatic tissue misdiagnosed as a tumor of lung. *Updates Surg.* 62:121–123. http://dx.doi.org/10.1007/s13304-010-0016-9

Vento, G., C. Tirone, P. Lulli, E. Capoluongo, F. Ameglio, S. Lozzi, F. Cota, F. Mosca, C. Romagnoli, I. Messana, et al. 2009. Bronchoalveolar lavage fluid peptidomics suggests a possible matrix metalloproteinase-3 role in bronchopulmonary dysplasia. *Intensive Care Med.* 35:2115–2124. http://dx.doi.org/10.1007/s00134-009-1646-6

Wallerman, O., M. Motallebipour, S. Enroth, K. Patra, M.S. Bysani, J. Komorowski, and C. Wadelius. 2009. Molecular interactions between HNF4a, FOXA2 and GABP identified at regulatory DNA elements through ChIP-sequencing. *Nucleic Acids Res.* 37:7498–7508. http://dx.doi.org/10.1093/nar/gkp823

Wan, H., S. Dingle, Y. Xu, V. Besnard, K.H. Kaestner, S.L. Ang, S. Wert, M.T. Stahlman, and J.A. Whitsett. 2005. Compensatory roles of Foxa1 and Foxa2 during lung morphogenesis. *J. Biol. Chem.* 280:13809–13816. http://dx.doi.org/10.1074/jbc.M414122200

Wang, S.J., P. Greer, and R. Auerbach. 1996. Isolation and propagation of yolk-sac-derived endothelial cells from a hypervascular transgenic mouse expressing a gain-of-function fps/fes proto-oncogene. *In Vitro Cell. Dev. Biol. Anim.* 32:292–299. http://dx.doi.org/10.1007/BF02723062

Weaver, M., N.R. Dunn, and B.L. Hogan. 2000. Bmp4 and Fgf10 play opposing roles during lung bud morphogenesis. *Development.* 127:2695–2704.

Yao, J., P.J. Guihard, A.M. Blazquez-Medela, Y. Guo, J.H. Moon, M. Jumabay, K.I. Boström, and Y. Yao. 2015. Serine protease activation essential for endothelial-mesenchymal transition in vascular calcification. *Circ. Res.* 117:758–769. http://dx.doi.org/10.1161/CIRCRESAHA.115.306751

Yao, J., P.J. Guihard, A.M. Blazquez-Medela, Y. Guo, T. Liu, K.I. Boström, and Y. Yao. 2016. Matrix Gla protein regulates differentiation of endothelial cells derived from mouse embryonic stem cells. *Angiogenesis.* 19:1–7. http://dx.doi.org/10.1007/s10456-015-9484-3

Yao, Y., A.F. Zebboudj, E. Shao, M. Perez, and K. Boström. 2006. Regulation of bone morphogenetic protein-4 by matrix GLA protein in vascular endothelial cells involves activin-like kinase receptor 1. *J. Biol. Chem.* 281:33921–33930. http://dx.doi.org/10.1074/jbc.M604239200

Yao, Y., S. Nowak, A. Yochelis, A. Garfinkel, and K.I. Boström. 2007. Matrix GLA protein, an inhibitory morphogen in pulmonary vascular development. *J. Biol. Chem.* 282:30131–30142. http://dx.doi.org/10.1074/jbc.M704297200

Yao, Y., A. Shahbazian, and K.I. Boström. 2008. Proline and γ-carboxylated glutamate residues in matrix Gla protein are critical for binding of bone morphogenetic protein-4. *Circ. Res.* 102:1065–1074. http://dx.doi.org/10.1161/CIRCRESAHA.107.166124

Yao, Y., M. Jumabay, A. Wang, and K.I. Boström. 2011. Matrix Gla protein deficiency causes arteriovenous malformations in mice. *J. Clin. Invest.* 121:2993–3004. http://dx.doi.org/10.1172/JCI57567

Yao, Y., M. Jumabay, A. Ly, M. Radparvar, A.H. Wang, R. Abdmaulen, and K.I. Boström. 2012. Crossveinless 2 regulates bone morphogenetic protein 9 in human and mouse vascular endothelium. *Blood.* 119:5037–5047. http://dx.doi.org/10.1182/blood-2011-10-385906

Yao, Y., M. Jumabay, A. Ly, M. Radparvar, M.R. Cubberly, and K.I. Boström. 2013a. A role for the endothelium in vascular calcification. *Circ. Res.* 113:495–504. http://dx.doi.org/10.1161/CIRCRESAHA.113.301792

Yao, Y., J. Yao, M. Radparvar, A.M. Blazquez-Medela, P.J. Guihard, M. Jumabay, and K.I. Boström. 2013b. Reducing Jagged 1 and 2 levels prevents cerebral arteriovenous malformations in matrix Gla protein deficiency. *Proc. Natl. Acad. Sci. USA.* 110:19071–19076. http://dx.doi.org/10.1073/pnas.1310905110

Zebboudj, A.F., M. Imura, and K. Boström. 2002. Matrix GLA protein, a regulatory protein for bone morphogenetic protein-2. *J. Biol. Chem.* 277:4388–4394. http://dx.doi.org/10.1074/jbc.M109683200

Zhou, L., C.R. Dey, S.E. Wert, C. Yan, R.H. Costa, and J.A. Whitsett. 1997. Hepatocyte nuclear factor-3β limits cellular diversity in the developing respiratory epithelium and alters lung morphogenesis in vivo. *Dev. Dyn.* 210:305–314. http://dx.doi.org/10.1002/(SICI)1097-0177(199711)210:3<305::AID-AJA10>3.0.CO;2-9